Desalination and Water Treatment
www.deswater.com

doi: 10.5004/dwt.2017.21457

92 (2017) 222–244
October

Mono/competitive adsorption of hexavalent chromium and acid fuchsin dye onto bamboo charcoal modified by Cu^{2+}-N-aminopropylsilane complexes via response surface methodology

Yunhai Wu[a,*], Haitao Sha[b], Yiang Fan[b]

[a]*Key Laboratory of Integrated Regulation and Resources Development of Shallow Lakes, Ministry of Education, Hohai University, Xikang Road #1, Nanjing 210098, China, Tel./Fax: +86 25 83786697; email: shthhu@163.com*
[b]*College of Environment, Hohai University, Xikang Road #1, Nanjing 210098, China, emails: 951666505@qq.com (H. Sha), 2659574450@qq.com (Y. Fan)*

Received 25 May 2017; Accepted 16 September 2017

ABSTRACT

The adsorption of acid fuchsin (AF) and hexavalent chromium [Cr(VI)], using Cu^{2+} and 3-aminopropyltrimethoxysilane modified bamboo charcoal (BC/Cu-N) as adsorbent, was investigated in single and binary systems. BC and the BC/Cu-N were characterized by Fourier-transform infrared spectroscopy, X-ray diffraction, scanning electron microscopy and energy-dispersive X-ray spectroscopy. The response surface methodology with four independent parameters (pH, initial concentration, adsorbent dosage and temperature) was used to optimize the adsorption process. The results showed that the maximum adsorption capacity of BC/Cu-N for AF and Cr(VI) was 13.6675 and 9.4000 mg/g, respectively. Besides, the adsorption data were more suitable for the Sips isotherm model in single system. The pseudo-second-order model could better describe the adsorption process both in the single and binary systems, and the external model and intraparticle diffusion were identified as the rate controlling steps. In the binary system, the removal of Cr(VI) was enhanced in the presence of AF, whereas the adsorption of AF was hindered by the presence of Cr(VI). Furthermore, the extended Freundlich multicomponent isotherm model was more appropriate for the simulation of adsorption data corresponding to AF and Cr(VI).

Keywords: Bamboo charcoal; Response surface methodology; Binary system; Adsorption; Isotherm model

1. Introduction

Numerous environmental problems occur with the industrial development and the progress of human civilization. Over the past decade, large amounts of pollutants were discharged into the environmental system, especially the aqueous environment, negatively impacting the overall quality of life of people. Contaminants are divided into two main categories, namely, inorganic and organic. As inorganic pollutants, heavy metals are considered hazardous, owing to their toxicity or carcinogenicity. Besides, heavy metals can easily accumulate in the human body, causing various diseases and even death. As one of the most common heavy metal ions, hexavalent chromium [Cr(VI)] is widely used in leather tanning, electroplating, cement manufacturing and so on [1,2]. It has become a problem in the disposal of industrial water, due to its hypertoxicity associated with chemical migration [3]. Part of the organic pollutants, much attention has been paid to dye wastewater, because of difficulties with its degradation. Dyes are used in many industries, such as textiles, rubber, paper, plastics and cosmetics [4]. The presence of dye in water can reduce light penetration, thus, affect the photosynthetic activity of aquatic life [5]. Moreover, several kinds of dyes are considered carcinogenic or mutagenic in humans. Hence, environmental regulations require the treatment of water, to remove heavy metals and dyes.

* Corresponding author.

At present, metals and dyes are removed separately. For the removal of heavy metals, frequently used methods include chemical precipitation [6], membrane filtration [7] and ion exchange [5,8,9]. Dzyazko et al. [10] developed ceramic membrane containing ion exchange components, such as zirconium dioxide, to remove Cr(VI) from waste water, and observed that the separation efficiency of the membrane increased with the increase in ion exchange components, whereas the increase in H^+ concentration would increase the separation rate of Cr(VI); Wang et al. [11] utilized a strongly basic ion-exchange resin for Cr(VI) removal in solution, and Khandegar and Saroha [12] introduced a method based on electrocoagulation to treat industrial effluent, including heavy metal ions. For the removal of dyes, various treatments have been employed, including chemical coagulation/flocculation, ozonation [13], oxidation and irradiation. Specifically, Song et al. [14] researched the degradation of Reactive Red 195 via an electrochemical method, using Ti/SnO_2-Sb/PbO_2 as electrode. Tehrani-Bagha et al. [15] investigated the effect of ozone on the decolorization and degradation of Active Blue 19, as well as the influencing factors, such as pH, dye concentration and electrolyte. Moreover, Wang et al. [16] employed the new type of *Enterobacter* sp. EC3 to dispose of dye waste water containing Active Black 5. However, in practice, waste water usually contains both metals and organic dye molecules, so their removal should occur simultaneously. Conventional solutions, such as the methods described above, are only valid for the removal of individual pollutants. However, as contaminants coexist, the non-targeted molecules may restrain the removal reaction. Compared with the aforementioned treatment methods, the purpose of adsorption is to cause the attachment of the pollutant to the adsorbent, which is a physical reaction process and is less affected by the interaction between metal ions and dye molecules. Moreover, the advantages of adsorption, such as simple design, easy operation [17] and low cost [18], are the important considerations in the final selection.

Bamboo charcoal (BC) is produced by the pyrolysis of bamboo [19], which is widely abundant in nature. BC is a type of porous medium material, with large specific surface area. These features make BC an ideal adsorbent, with great adsorption potential in environmental protection, medical industry, food industry and other fields [20]. To improve the adsorption capacity of BC, many authors adopted suitable methods to modify the physical and chemical properties of its surface. For example, Wang et al. [21] obtained a kind of BC which loaded nickel, through the pyrolysis of *Phyllostachys bambusoides* in the presence of oxygen. After the analysis of representation, the BC had a higher specific surface area and pore volume, and the corresponding adsorption efficiency was improved. Fan et al. [22] employed NaOH to modify BC in order to dispose of aqueous chloramphenicol, and demonstrated that the modification could increase the number of functional groups containing oxygen on charcoal surface, and thus improve its adsorption capacity. Jain et al. [23] reported the reaction process of grafting different kinds of transition metals (Fe^{3+}, Co^{2+}, Ni^{2+} and Cu^{2+}) onto MCM-41 (Mobil Composition of Matter No. 41), followed by the application of modified MCM-41 in adsorption. The results showed that the modification induced by the transition metals could enhance the adsorption capacity of MCM-41.

The aim of this work was to investigate the ability of BC, modified by Cu^{2+} and 3-aminopropyltrimethoxysilane, to remove Cr(VI) and AF from single and binary component systems. Multiple parameters (pH, initial concentration, adsorbent dosage, temperature) were optimized for maximum removal efficiency by response surface methodology (RSM) [24,25]. The adsorbent was characterized by Fourier-transform infrared spectra (FTIR), X-ray diffraction (XRD), scanning electron microscopy (SEM) and energy-dispersive X-ray spectroscopy (EDS). Isotherm and kinetic parameters were calculated to determine the adsorption mechanism.

2. Materials and methods

2.1. Preparation of modified bamboo charcoal

BC was broken into small blocks and dried at 105°C for 24 h. Subsequently, BC was boiled for 30 min in the distilled water and cooled to room temperature, then ground and screened through a 60-mesh sieve, before undergoing further modification.

0.5 g of $CuSO_4 \cdot 5H_2O$ and 3 g of 3-aminopropyltrimethoxysilane (the molar ratio for $CuSO_4 \cdot 5H_2O$ and 3-aminopropyltrimethoxysilane was 1:2) were added to 50 mL of *n*-hexane, and the mixture was then stirred for 30 min. After this, 3 g of prepared BC was added to the solution, and magnetically stirred for 17 h. The mixture was rinsed with ultrasonic treatment after being washed in distilled water multiple times. Afterwards, the BC powder was filtrated, and dried at 102°C for 24 h. At last, the obtained adsorbent was called Cu^{2+}-N-aminopropyltrimethoxysilane complexes (BC/Cu-N) [25]. All other chemicals used in this study were of analytical grade.

2.2. Characterization of BC and BC/Cu-N

To analyze the chemical properties of BC before and after being modified, FTIR (Bruker, Germany) was obtained, with all spectra recorded between 4,000 and 400 cm^{-1}. Besides, the crystalline phases of BC and BC/Cu-N were examined using XRD (ARL Corporation, Switzerland), with the 2θ ranging from 10 to 80°. The surface morphology of the adsorbent before and after modification was characterized by SEM (S4800, Hitachi, Japan) and element composition was analyzed by EDS (S4800, Hitachi, Japan).

2.3. Preparation of acid fuchsin and Cr(VI) solution

Stock solutions of 100 mg/L of AF and Cr(VI) were prepared by dissolving appropriate amounts of AF and K_2CrO_7 in distilled water. Working solutions were prepared by suitable dilution of the stock solutions. Adjustment of pH was carried out using 0.1 M NaOH or 0.1 M HCl. The concentrations of AF and Cr(VI) were determined using UV1201 (Rayleigh, China), at the wavelengths of 524 and 540 nm, respectively.

2.4. Adsorption experiments

2.4.1. Adsorption in a single component system

Batch adsorption experiments designed by RSM were conducted in a reaction mixture of certain amounts of

BC/Cu-N and 50 mL of solution containing AF or Cr(VI) to study the effect of preselected operating variables on adsorption of AF or Cr(VI). The experiments were performed in a shaker at 140 rpm, for 3 h. After that, the reaction mixture was filtered. The initial and finial AF and Cr(VI) concentrations were measured by ultraviolet spectrophotometer.

2.4.2. Adsorption in a binary component system

The binary experiments were conducted with 0.04 g BC/Cu-N and 50 mL Cr(VI) solution (8 mg/L) in 250 mL conical flasks, at 40°C, in the presence of AF solution at 4, 8 and 12 mg/L, respectively. And vice versa, 0.04 g BC/Cu-N were added into 50 mL AF solution (8 mg/L), which also contained Cr(VI) solution at 4, 8 and 12 mg/L, respectively. The effect of pH on the adsorption system was investigated in the range of 2–9. Then, the mixture was agitated on a temperature-controlled shaker, at the speed of 140 rpm, for 3 h. The solution mixture was measured for the concentrations of AF and Cr(VI) after being filtered, when the reaction reached the equilibrium.

The removal percentage and adsorption capacity (q_e) were calculated by using the following equation:

$$\text{Removal}\ (\%) = \frac{(C_0 - C_e)}{C_0} \times 100\% \quad (1)$$

$$q_e = \frac{(C_0 - C_e) \cdot V}{M} \quad (2)$$

where C_0 (mg/L) and C_e (mg/L) are the initial and finial concentration of AF and Cr(VI) in the solution, respectively. V (mL) is the volume of solution and M (g) is the mass of adsorbent. All batch study experiments were conducted in duplicate and only the average value was used.

2.5. Response surface methodology

RSM is a collection of statistical and mathematical techniques which was useful for developing, improving, and optimizing process. The main objective of it was to decide the optimal operational conditions for systems and to determine the region that satisfies the operating specifications [20]. The main advantage of RSM is to reduce the number of experimental trials needed to assess multiple parameters and their interactions. The RSM has widely been applied in chemical engineering and sorption process optimization.

The central composite design (CCD), a widely used form of RSM, was selected in this study to explore the optimum condition of AF and Cr(VI) by BC/Cu-N. A set of four independent variables (pH (A), initial concentration (B), adsorbate dosage (C), temperature (D)) was identified to investigate their effect on the removal process. At the same time, the range and center point values of four variables were selected based on the preliminary experiments and displayed in Tables 1 and 2. A second-order polynomial regression model equation (Eq. (3)) was evaluated here to predict the removal efficiency under a certain condition of process variables [26,27]:

Table 1
Independent variables and their coded levels for the central composite design on AF adsorption

Factors		Range of actual and coded variables				
		–2	–1	0	1	2
pH	A	2	4	6	8	10
Initial AF concentration (mg/L)	B	4	6	8	10	12
Adsorbent dosage (g)	C	0.02	0.03	0.04	0.05	0.06
Temperature (°C)	D	30	35	40	45	50

Table 2
Independent variables and their coded levels for the central composite design on Cr(VI) adsorption

Factors		Range of actual and coded variables				
		–2	1	0	1	2
pH	A	2	4	6	8	10
Initial Cr(VI) concentration (mg/L)	B	2	4	6	8	10
Adsorbent dosage (g)	C	0.03	0.04	0.05	0.06	0.07
Temperature (°C)	D	30	35	40	45	50

$$Y(\%) = a_0 + \sum_{i=1}^{n} a_i X_i + \sum_{i=1}^{n} a_{ii} X_i^2 + \sum_{i=1}^{n-1} \sum_{j=2}^{n} a_{ij} X_i X_j + e \quad (3)$$

where a_0 is the constant coefficient, a_i, a_{ii}, and a_{ij} are the regression coefficient and X_i, X_j indicate the independent variables in the form of coded values, and e is the random error [28]. The regression coefficient was then used to make statistical calculation to generate dimensional and contour maps from the regression models.

A total of 30 groups of trials obtained from Design Expert software were presented in Tables S1 and S2 (ESI). After the formation of a 2^4 CCD model, the statistical significance of the regression coefficient was tested using analysis of variance (ANOVA). Moreover, the optimum values of the selected variables were obtained by solving the regression equation and analyzing the response surface plots.

3. Results and discussion

3.1. Characterization of BC/Cu-N

The FTIR spectra of BC, AF-adsorbed BC/Cu-N and Cr(VI)-adsorbed BC/Cu-N are illustrated in Fig. 1(a). According to the FTIR spectra, the peaks of 2,361 and 2,363; 1,699 and 1,636; and 1,065 and 1,111 cm^{-1} correspond to the stretching vibrations of the C=N, C=O and C–O bonds, respectively. The amount of the corresponding functional groups might change with the shift in intensity and site of the corresponding peaks. The peak of 1,558 cm^{-1} indicates that the C=C was present in the spectra of BC, but not observed in that of BC/Cu-N, which illustrated that the functional groups C=C were destroyed

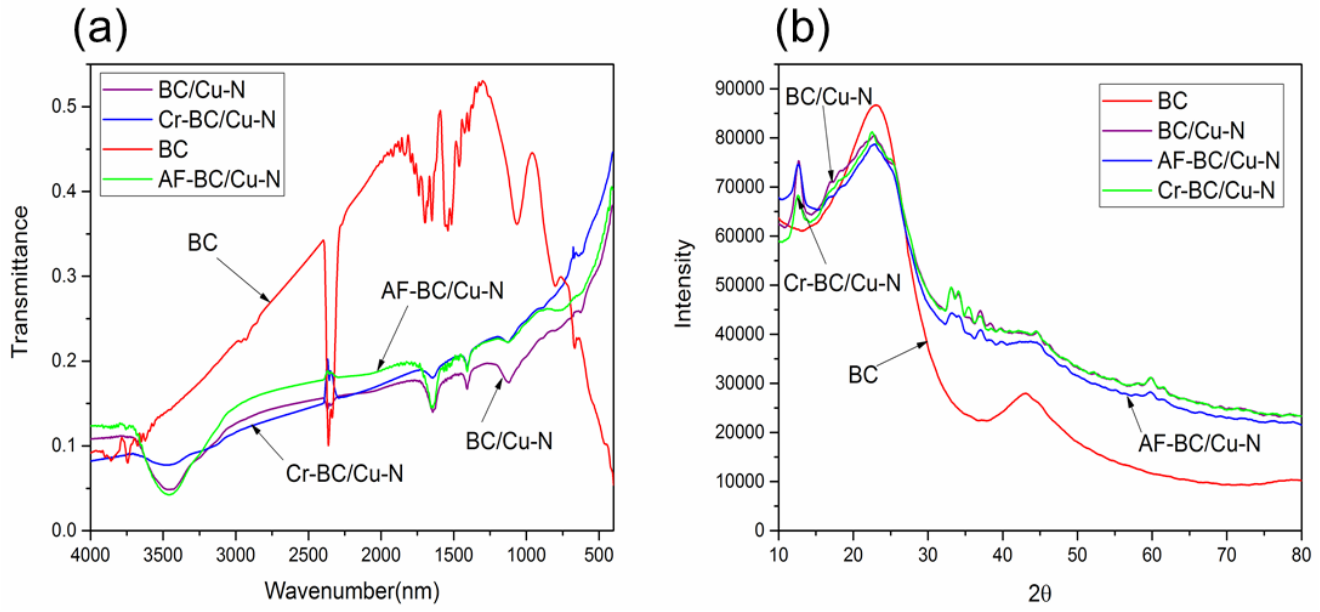

Fig. 1. FTIR spectra (a) and XRD patterns (b) of BC, BC/Cu-N, AF-BC/Cu-N and Cr-BC/Cu-N.

during the modification. The peak of 3,462 cm^{-1} was attributed to the O–H group, which largely proved the existence of little water. Moreover, according to the peak of 1,400 cm^{-1}, which represents the existence of amino acid salts, it can be assessed that $CuSO_4$ and 3-aminopropyltrimethoxysilane were loaded on the BC when the measurement was performed [29]. From Fig. 1(a), the characteristic peaks of functional groups on the adsorbent surface did not move, but the peak strength weakened. It indicated the corresponding functional groups participated in the sorption reaction, leading to the decrease in the number of groups and the enhancement of light transmittance [30].

The XRD patterns are shown in Fig. 1(b). From Fig. 1(b), the two strong peaks at 22.8° and 42.8° are associated with the crystal plane at peaks (002) and (100) of activated carbon materials, indicating the low graphitization degree and amorphous structure of BC. The intensity of the diffraction peak was reduced by a little, but the sites of the peaks did not change. BC had the obvious peak in the angle of 22.8° after the modification with the complex of Cu-N, and this phenomenon indicates that the structure of BC was not destructed and the disorder of the structure was increased to some extent. Moreover, the surface of BC/Cu-N appeared new, with only faint peaks in the angles of 33.1°, 37.2° and 59.8°, which may have resulted from the loading of complex of Cu-N. After the adsorption by the BC/Cu-N, the diffraction peak (002) in the angle of 22.8° was still present at the same site, but with decreased strength. Therefore, this suggests that the adsorption reaction did not destroy the structure of the adsorbent.

The SEM images are shown in Fig. 2. The graph displaying the surface of BC was generally smooth, presenting some micro-pores (Fig. 2(a)). In contrast, Fig. 2(b) shows that the BC/Cu-N had a rough surface and abundant holes, which favored the adsorption reaction. As can be seen in Figs. 2(c) and (d), the SEM images for BC/Cu-N after adsorption had some additional crumbs or small granular material than before sorption, which suggests that the adsorbate was successfully adsorbed on the surface of adsorbent. The corresponding EDS spectra of BC, BC/Cu-N and Cr(VI)-BC/Cu-N are given in Fig. S1 (EIS). The analysis of the EDS corresponding to BC before modification indicated the main components of BC were C and O (Fig. S1(a) (EIS)). Moreover, the Fig. S3(b) (EIS) revealed the major ingredients of BC/Cu-N were C, O, Cu, and a little Si and S. This indicates that Cu, Si and S were grafted onto the BC due to the modification. In contrast with Fig. S3(b) (EIS), Fig S3(c) (EIS) shows the BC/Cu-N after adsorption had one more element than that before, which was chromium. The detection of chromium proved that the Cr(VI) molecules successfully stuck to the adsorbent.

The back-titration curves of BC/Cu-N and blank experiment are displayed in Fig. S2 (EIS). The back-titration process of BC/Cu-N consumed more NaOH solution than blank experiment and the buffer was observed in the back-titration curves of BC/Cu-N. It indicates that not only did the H^+ in solution react with the added OH^- but also that there were substances ($M\text{-}OH_2^+$) which could consume the OH^- ions present on the surface of BC/Cu-N. In contrast, in the blank sample, the OH^- only reacted with H^+ in solution, to adjust the solution pH. The amount of acid, alkali and pH used in titration were all recorded. Then, the pH in titration point, total concentration of H^+ after the experiment and the concentrations at active sites of BC/Cu-N were calculated by the Gran plot equations, which were described as follows [31]:

$$\text{On the acidic side}: G_a = \left(V_0 + V_a + V_b\right) \times 10^{-\text{pH}} \times 100 \quad (4)$$

$$\text{On the alkaline side}: G_a = \left(V_0 + V_a + V_b\right) \times 10^{-(13.8-\text{pH})} \times 100 \quad (5)$$

where V_0 represents the initial volume of the suspension; V_a and V_b are the total volume of acid solution and the volume of NaOH used in titration at each point, respectively; the intersection points of the Gran plot with the X axis are V_{eb1} and V_{eb2}, which correspond to V_{eb1} and V_{eb2} of the blank

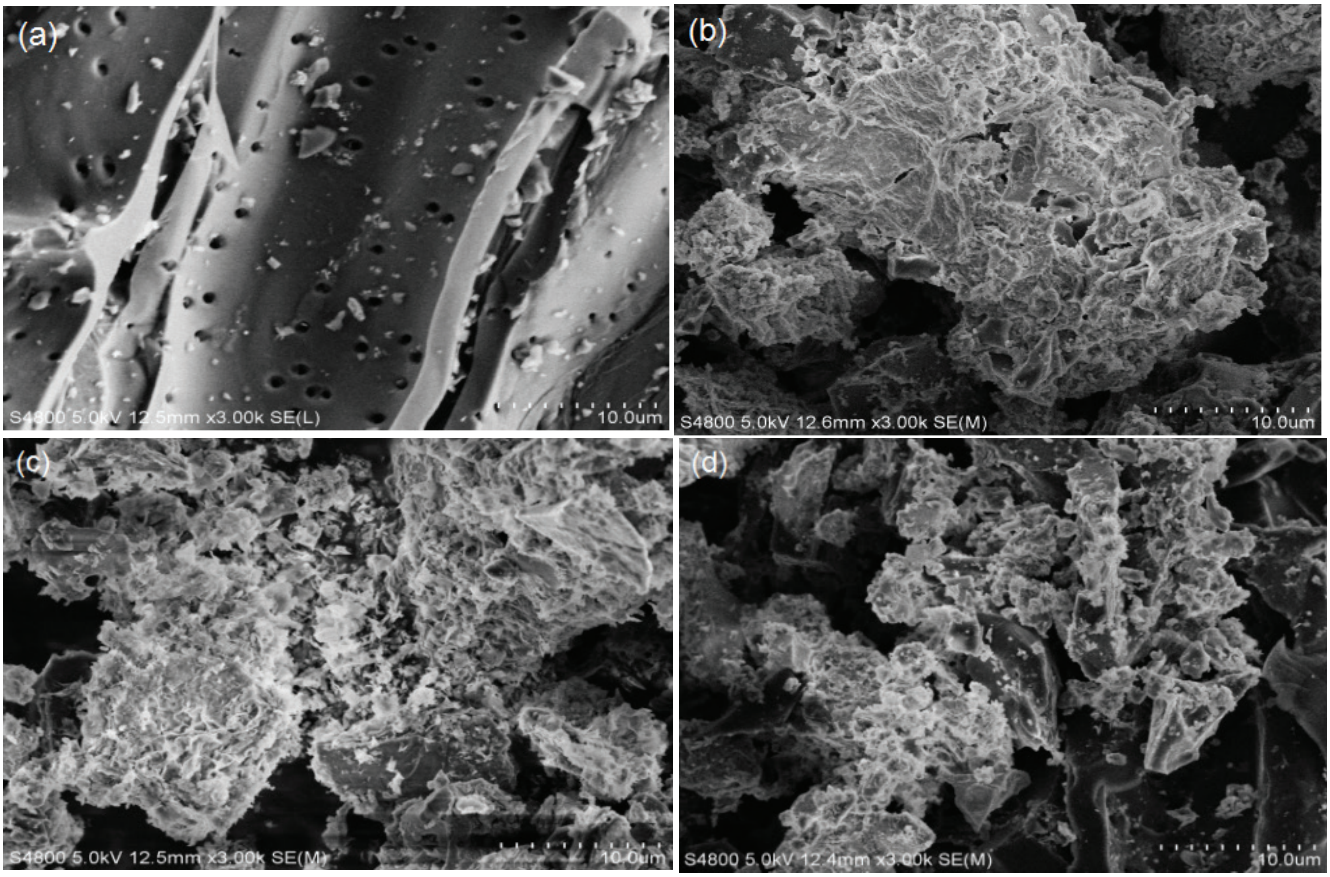

Fig. 2. SEM images of BC (a), BC/Cu-N (b), Cr-BC/Cu-N (c) and AF-BC/Cu-N (d).

experiment, respectively. The concentration of active sites was obtained by calculating the adsorption capacity of H^+ on the surface of BC/Cu-N [32], as shown:

$$H_s = \frac{\left(V_{eb2} - V_{eb1}\right) \times C_b - \left(V'_{eb2} - V'_{eb1}\right) \times C_b}{V_0} \quad (6)$$

Gran plots of BC/Cu-N and blank experiment, during the back-titration process, are illustrated in Fig. 3(a). This shows that the titration process of NaOH can be divided into three steps, including the consumption of excess H^+ from the acid titration (before V_{eb1}), contributing to the pH value of the system (after V_{eb2}), and reacting with the solid surface of BC/Cu-N (between V_{eb1} and V_{eb2}). The consumption of proton total concentration in every titration point was calculated via the following equation:

$$\mathrm{TOTH} = \frac{-\left(V_b - V_{eb1}\right) \times C_b}{V_0 + V_b} \quad (7)$$

where C_b is the concentration of NaOH, V_{eb1} is the volume of NaOH used in titration at Gran point, to zero at acidic side. The titration curve of TOTH vs. pH plot is shown in Fig. 3(b). When the TOTH value is zero, the zero point of charge is the beginning of the deprotonation stage, derived from the protonation stage. Hence, the pH_{pzc} value of BC/Cu-N was calculated to be 6.2.

3.2. Comparison of removal efficiencies of BC, BC/N and BC/Cu-N

To highlight the adsorption capacity of BC after modification for Cr(VI) and AF, the different removal efficiencies of the three kinds of adsorbents (BC, BC/N and BC/Cu-N) for Cr(VI) and AF were researched. The adsorption of Cr(VI) by the three adsorbents is illustrated in Fig. S3(a) (EIS). It is obvious that the adsorption of BC for Cr(VI) was the lowest, and even though the BC was modified by 3-aminopropyltrimethoxysilane, its adsorption capacity (23.79%) was still lower than that of BC/Cu-N (69.93%). This indicates that the modifications induced by Cu^{2+}-3-aminopropyltrimethoxysilane or 3-aminopropyltrimethoxysilane can increase the adsorption capacity for Cr(VI). Compared with 3-aminopropyltrimethoxysilane, the addition of Cu^{2+} can further enhance the adsorption process, which may be due to that the graft of 3-aminopropyltrimethoxysilane can produce the corresponding amino group on the surface of BC which can chelate the metal ions [33,34], while the BC/Cu-N not only contained the amino group on the surface but also generated amino acid salts, due to the presence of Cu^{2+}. Cu^{2+} might undergo ion exchange with metal ions to facilitate the adsorption process. As shown in Fig. S3(b) (EIS), both the BC/N (21.34%) and BC/Cu-N (86.22%) had higher removal efficiencies for AF than BC, indicating that the modification can improve the adsorption capacity of BC for AF. This was consistent with the graph, which also demonstrated that the BC/Cu-N had the highest removal efficiency.

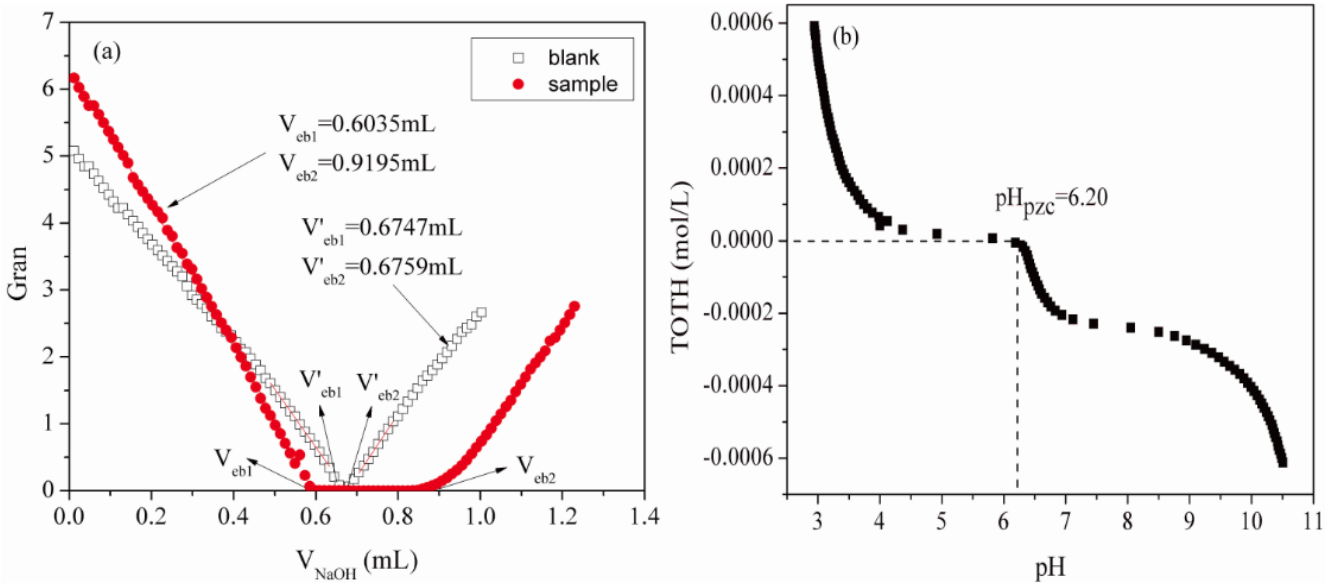

Fig. 3. Gran plot of BC/Cu-N (a) and corresponding TOTH–pH plot of BC/Cu-N (b).

3.3. Statistical analysis and model fitting

RSM has more advantages than traditional single parameter optimization in that it saves time, space and raw materials [35]. There were just 30 runs for optimizing the four individual parameters in the current CCD. To optimize the response surface, an appropriate fit of the model was obtained, to avoid useless or ambiguous results. The second-order polynomial model was advisable for both responses, based on the sequential model sum of squares, in which the additional terms were significant and the models were not aliased. The second-order polynomial model for estimating the removal efficiency of AF and Cr(VI) was, respectively, shown in Eqs. (8) and (9), with insignificant terms excluded:

$$\begin{aligned} q_e(C_r) = {} & 5.44 - 0.004956 \times A + 1.97 \times B - 1.05 \times C \\ & + 0.022 \times D - 0.08 \times A \times B + 0.078 \times A \times C \\ & - 0.055 \times A \times D - 0.37 \times B \times C - 0.042 \times B \times D \\ & + 0.002344 \times C \times D - 0.093 \times A^2 + 0.007496 \times B^2 \\ & + 0.22 \times C^2 + 0.012 \times D^2 \end{aligned} \quad (8)$$

$$\begin{aligned} q_e(AF) = {} & 7.71 + 0.031 \times A + 1.90 \times B - 1.64 \times C \\ & + 0.16 \times D - 0.12 \times A \times B + 0.037 \times A \times C \\ & + 0.044 \times A \times D - 0.22 \times B \times C + 0.036 \times B \times D \\ & - 0.053 \times C \times D - 0.38 \times A^2 - 0.16 \times B^2 \\ & + 0.43 \times C^2 + 0.082 \times D^2 \end{aligned} \quad (9)$$

The results of ANOVA on the adsorption experiment were listed in Table 3. As can be seen, the values of F in the RSM model were 39.57 for AF and 134.23 for Cr(VI), which indicates that the second-order polynomials of AF and Cr(VI) were statistically significant. The large F value showed that there was only 0.01% chance that could happen due to error during the experiment and can describe the relationship between the variables and adsorption quantity. Both P values for AF and Cr(VI) were less than 0.001, so the statistical significance of model terms was demonstrated again.

The predicted vs. actual removal efficiency of AF and Cr(VI) is plotted in Fig. S4 (EIS). The actual and predicted values of removal efficiency were in agreement, providing evidence for the validity of the regression model as well. Besides, the values of R^2 and R^2_{adj} were assessed as 0.9736 and 0.9490 for AF removal, and 0.9921 and 0.9847 for Cr(VI) removal, respectively. These values were almost equal to 1, implying that the polynomial had a perfect fitting effect, so that it could be used for the experimental predictions. Furthermore, the value of A_{deq} precision was used to measure the signal of noise ratio, with a ratio greater than 4 being considered desirable. In this study, the values for AF and Cr(VI) were of 24.494 and 43.428, respectively. Both of them were much larger than 4, providing evidence for the reliability of the RSM model and its use in describing adsorption.

The three-dimensional (3D) response surface plots were generated to investigate the effects of four process parameters (pH, initial concentration, adsorbent dosage and temperature) on the adsorption of AF and Cr(VI) (Figs. 4(a)–(f) and 5(a)–(f)).

3.4. Single component system adsorption experiment

3.4.1. Effect of pH

The pH was an important variable in the metal adsorption process in that the variation of pH not only influenced the charge of adsorbent surface but also affected the ionic type or state of the metal. In this study, the effect of pH on Cr(VI) removal is depicted in Figs. 4(a), (e) and (f). The adsorption capacity of Cr(VI) did not markedly vary as the pH ranged from 4 to 8, which implies that the change of pH had little influence on the adsorption of Cr(VI). Considering the great influence of pH in the reaction process, Cr(VI) had different forms in solution at different pH values, so this study specially

Table 3
Analysis of variance (ANOVA) of the response surface quadratic for AF and Cr(VI) adsorption

Source	Sum of squares		df	Mean square		F-value		Probability > F	
	AF	Cr(VI)		AF	Cr(VI)	AF	Cr(VI)	AF	Cr(VI)
Model	164.75	123.53	14	11.77	8.82	39.57	134.23	<0.0001	<0.0001
A	0.023	5.917×10^{-4}	1	0.023	5.917×10^{-4}	0.07	9.001×10^{-3}	0.7855	0.9257
B	86.58	92.98	1	86.58	92.98	291.13	1414.50	<0.0001	<0.0001
C	64.84	26.38	1	64.84	26.38	218.01	401.37	<0.0001	<0.0001
D	0.63	0.011	1	0.63	0.011	2.13	0.17	0.1646	0.6833
AB	0.23	0.10	1	0.23	0.10	0.76	1.58	0.3968	0.2285
AC	0.022	0.097	1	0.022	0.097	0.075	1.48	0.7875	0.2432
AD	0.031	0.049	1	0.031	0.049	0.11	0.75	0.7502	0.4005
BC	0.78	2.14	1	0.78	2.14	2.64	32.49	0.1253	<0.0001
BD	0.021	0.029	1	0.021	0.029	0.071	0.44	0.7933	0.5179
CD	0.046	8.789×10^{-5}	1	0.046	8.789×10^{-5}	0.15	1.337×10^{-3}	0.7009	0.9713
A^2	4.03	0.23	1	4.03	0.23	13.56	3.57	0.0022	0.0782
B^2	0.70	1.53×10^{-3}	1	0.70	1.53×10^{-3}	2.35	0.023	0.1458	0.8808
C^2	5.07	1.31	1	5.07	1.31	17.06	19.93	0.0009	0.0005
D^2	0.19	4.264×10^{-3}	1	0.19	4.264×10^{-3}	0.63	0.065	0.4410	0.8024
Residual	4.46	0.99	15	0.30	0.066				
Lack of fit	4.27	0.73	10	0.43	0.073	10.90	1.44	0.0083	0.3595
Pure error	0.20	0.25	5	0.039	0.051				
Cor total	169.21	124.52	29						

design the adsorption trial of Cr(VI) alone affected the pH (Fig. S5(a) (EIS)) and the form distribution of Cr(VI) at different pH values are shown in Fig. S6 (EIS). From the diagram, Cr(VI) existed in solution in the form of oxyanions, such as $HCrO_4^-$, CrO_4^{2-} and $Cr_2O_7^{2-}$. The dominant form of Cr(VI) is $HCrO_4^-$ at lower pH (1–5). As the pH rises, the main species of Cr(VI) are CrO_4^{2-}, $Cr_2O_7^{2-}$, etc. [36–38]. Besides, the removal efficiency of Cr(VI) was almost the same at pH ranging from 4 to 7. The adsorption capacity of Cr(VI) had a short-lived, faster increase from 8.15 to 9.11 mg/g, with the pH ranging from 2 to 4. This could be explained by the electrostatic attraction between $HCrO_4^-$, which was main state of Cr(VI) at that pH, and the adsorbent, whose surface was protonated and positively charged at the pH lower than 6.20 (pH_{pzc}). Adsorption capacity reduced from 9.20 to 8.91 mg/g when pH increased from 7 to 9. This is because the pH is greater than 6.20 (pH_{pzc}), thus the surface of the adsorbent was deprotonated and carried negative charge, meanwhile, CrO_4^- was the major form of Cr at this pH (pH > 6.20). The electrostatic repulsion between adsorbent, whose surface was negatively charged, and CrO_4^- restrained the adsorption reaction. The rare change in adsorption capacity of Cr(VI) at pH values ranging from 4 to 7 could be attributed to that CrO_4^- was replacing $HCrO_4^-$ as the dominant form of Cr(VI), and the surface of adsorption was still protonated, hence, the electrostatic attraction of the surface and CrO_4^-/$HCrO_4^-$ maintained the ability of BC/Cu-N to adsorb the Cr(VI) in solution. Moreover, when pH was in range of 6.2–7, ion exchange between Cr(VI) and adsorbent also favored the adsorption of Cr(VI).

Figs. 5(a), (e) and (f) show the effect of pH on the removal of AF from the solution, and indicate that the pH ranging from 4 to 8 had little effect on the removal of AF. Even so, the AF adsorption quantity also slightly increased with higher pH value. To add the supplementary information on the effect, which only contained the variable pH, on the removal of AF, which was distinguished from the model, the obtained data are exhibited in Fig. S5(b) (EIS). As can be seen, the adsorption capacity increased sharply at low pH (4 > pH > 2), but when the pH value was higher than 6.20, the rate of the augment of the sorption efficiency was reduced, although still maintained an increasing trend. Low pH values of less than 6.20 increased the H^+ concentration in solution, then the adsorbent surface was positively charged through adsorption of H^+ ions. At the same time, the AF dye was decomposed into sodium ions (Na^+) and sulfonate anions, so the strong electrostatic attraction between the positively charged adsorbent surface and anion dye molecules could promote the adsorption of AF [39]. Furthermore, the pH (>6.20) had a negligible impact on the adsorption of AF, due to the repulsive force between the negatively charged surface and anion dye molecules. In contrast, Van der Waals forces present between adsorbent and dyes molecules facilitated the adsorption reaction [36,40].

3.4.2. Effect of initial concentration

The combined effects of initial concentration with pH, adsorbent dosage and temperature on adsorption of

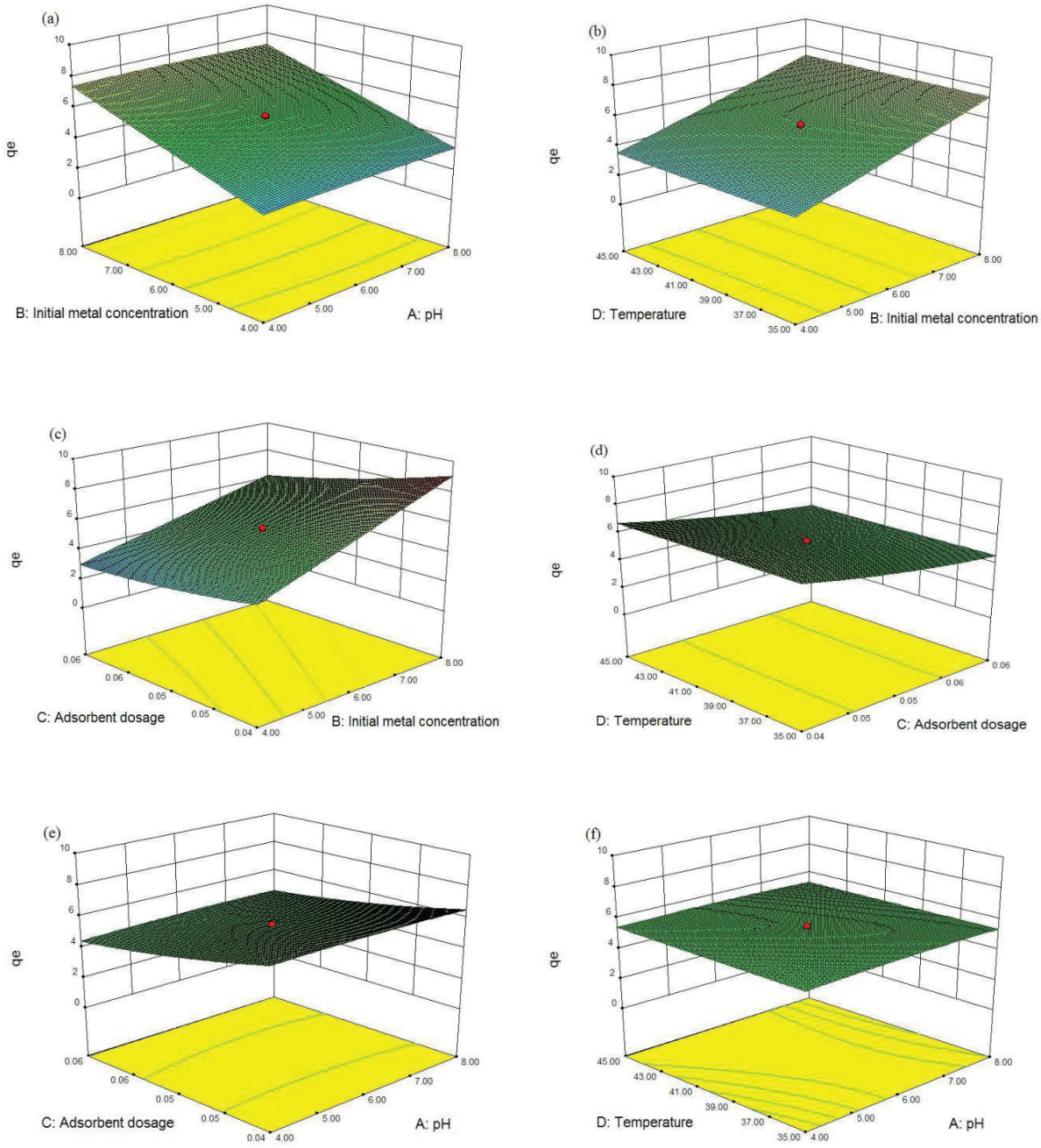

Fig. 4. Response surface (3D) showing the combined effect of (a) initial metal ion concentration and pH (adsorbent dosage 0.05 g, temperature 40°C), (b) initial metal ion concentration and temperature (adsorbent dosage 0.05 g, pH 6), (c) adsorbent dosage and initial metal ion concentration (pH 6 and temperature 40°C), (d) temperature and adsorbent dosage (pH 6 and initial metal ion concentration 6.0 mg/L), (e) pH and adsorbent dosage (temperature 40°C and initial metal ion concentration 6.0 mg/L), (f) temperature and pH (initial metal ion concentration 6.0 mg/L and adsorbent dosage 0.05 g) on Cr(VI) removal.

Cr(VI) and AF are shown in Figs. 4(a)–(c) and 5(a)–(c). It can be observed that the removal capacity of AF and Cr(VI) increased with the increasing initial concentration, at limited adsorbent dosage. This was because the quantified amount of adsorbent had limited active adsorption sites, and when the initial concentrations of AF and Cr(VI) were low, the metal ions and dye molecules could not occupy the adsorption sites entirely, thus, the adsorbent did not reach saturation and the adsorption efficiency was relatively lower. Actually, as the initial concentration increased, the concentration gradient on the contact surface between solution and adsorbent became greater, which helps the metal ions and dye molecules to overcome the resistance to attach to the adsorbent surface and increases the probability of collision between metal ions, dye molecules and effective adsorption sites, increasing the adsorption efficiency of AF and Cr(VI) [41].

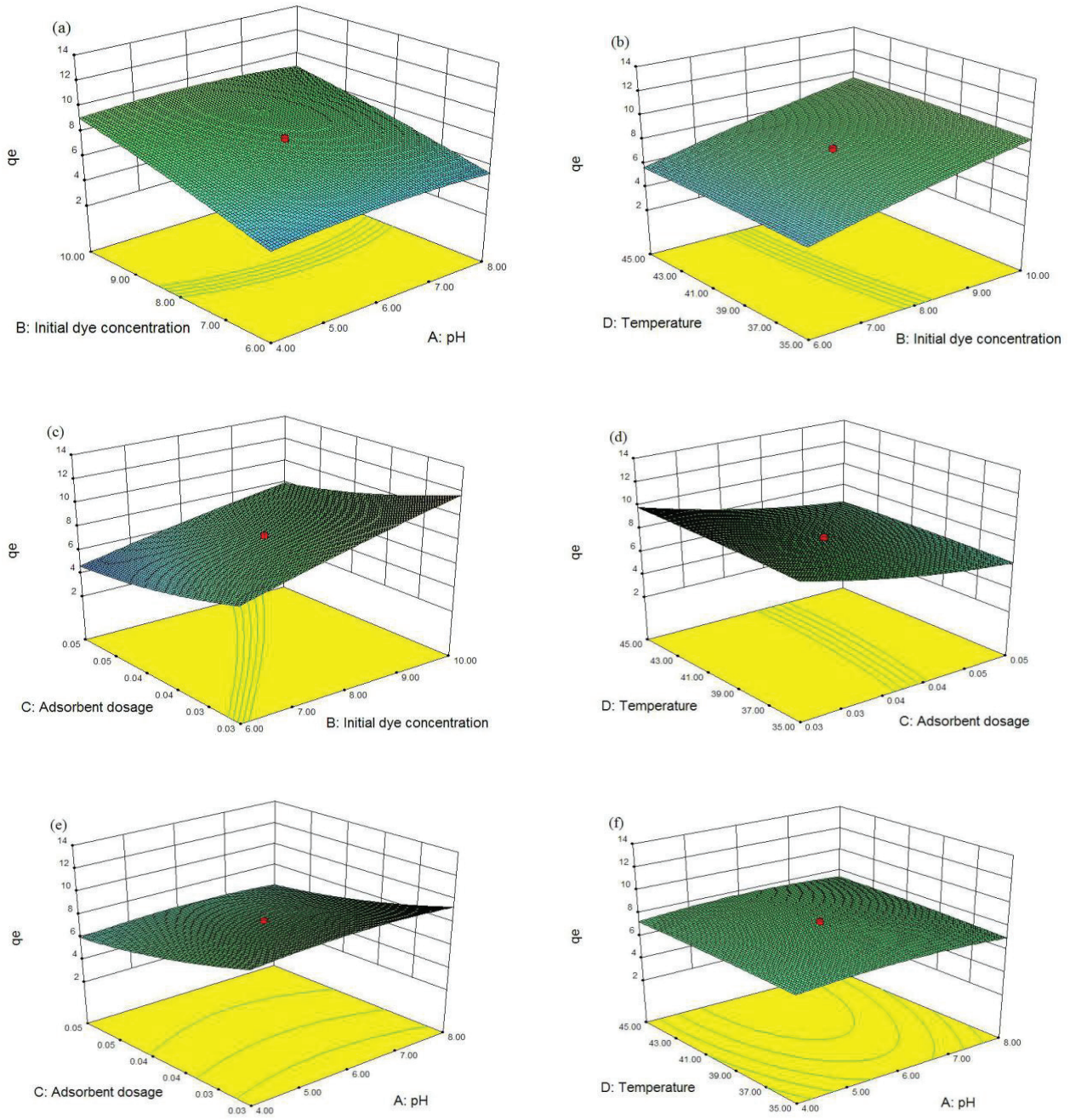

Fig. 5. Response surface (3D) showing the combined effect of (a) initial dye concentration and pH (adsorbent dosage 0.04 g, temperature 40°C), (b) initial dye concentration and temperature (adsorbent dosage 0.04 g, pH 6), (c) adsorbent dosage and initial dye concentration (pH 6 and temperature 40°C), (d) temperature and adsorbent dosage (pH 6 and initial dye concentration 8.0 mg/L), (e) pH and adsorbent dosage (temperature 40°C and initial dye concentration 8.0 mg/L), (f) temperature and pH (initial dye concentration 8.0 mg/L and adsorbent dosage 0.04 g) on AF removal.

3.4.3. Effect of adsorbent dosage

The effect of adsorbent dosage on Cr(VI) and AF removal is depicted in Figs. 4(c)–(e) and 5(c)–(e). These diagrams show that removal efficiency decreased with increase in adsorbent dosage at a fixed concentration of Cr(VI) and AF. When the adsorption process achieved a balance, the remnant concentrations of Cr(VI) and AF were lower than before, which resulted in the decrease of pressure of concentration gradient from residual metal ions and dye molecules. Consequently, the driving force supplied by pressure of concentration gradient was insufficient and could not overcome the transfer resistance of the solution. Thus, the adsorption capacity did not increase as the amount of adsorbent increased. In addition, the possibility of aggregation of adsorbent increased

with the increase of adsorbent dosage, which reduced the specific surface area and the effective adsorption sites on the surface, which was one of the reasons for the observed decrease in adsorption capacity.

3.4.4. Effect of temperature

The effect of temperature on the adsorption of Cr(VI) and AF on BC/Cu-N is displayed in Figs. 4(b), (d), (f) and 5(b), (d), (f). In general, the removal efficiency increased with the increasing temperature, though only slightly, which indicates that the adsorption of Cr(VI) and AF was an endothermic reaction. Meanwhile, the high temperature could cause the slight dilation of BC/Cu-N, which also increased the pore diameter and volume of adsorbent. Moreover, the activity of AF molecules and Cr(VI) ions was strengthened by higher temperatures and which produced a faster speed of movement in solution [42]. As a result, there were more adsorbate molecules reaching the adsorbent surface through the outer diffusion layer of the adsorbent [42].

3.5. Binary component system adsorption experiment

3.5.1. Cr(VI) adsorption in the presence of AF at different pH

The simultaneous adsorption of Cr(VI), from binary mixtures at different pH, is investigated in Fig. 6(a). The molar mass proportions of Cr(VI) and AF were 2:1, 1:1 and 1:2. The diagram showed that the effect of pH on the adsorption of Cr(VI) in the binary system was similar to that in the single system. As can be seen, the removal efficiency of Cr(VI) increased with the decrease of the proportion of Cr(VI) and AF. The presence of AF promoted the adsorption of Cr(VI). This was due to the AF molecules and chromate ions generating a kind of complex on the surface of BC/Cu-N, which could facilitate the adsorption reaction. However, an excessive amount of AF may generate a substance with the chromate ions in solution, which can lead to the stabilization of the chromate ions in the solution. And, while the concentration of AF was increased, the agglomeration of the complex product occurred [43], which may lead to the decrease in the adsorption capacity of Cr(VI).

3.5.2. AF adsorption in the presence of Cr(VI) at different pH

The mutual effect of pH combined with the presence of Cr(VI), on the removal of AF is quantitatively demonstrated in Fig. 6(b). The molar ratios of AF and Cr(VI) were 2:1, 1:1 and 1:2. From the chart, the adsorption capacity of AF in the binary system was lower than that in the single system, and the reduction in AF adsorption was enhanced by the increase in Cr(VI) concentration in the mixed solution. This illustrates that the chromate ions competed with AF, occupying the adsorption sites of BC/Cu-N. Besides, the Cr(VI) and the functional groups on the adsorbent produced compounds via external complexation reaction, forming a tight water film, which can inhibit the hydrophilic or hydrophobic functional groups on the surface of the adsorbent, decreasing the adsorption capacity indirectly [44].

3.6. Adsorption isotherms

Equilibrium isotherm analysis provided fundamental physicochemical data about the reaction process. The maximum adsorption capacity could also be obtained from the isotherms. In this study, Langmuir [45], Freundlich [46], D-R [47] model and Sips [48] isotherm models were applied to describe the equilibrium.

The Langmuir isotherm model assumes a monolayer adsorption and insists that the interaction force between adsorbed molecules is negligible:

$$q_e = \frac{q_m K_L C_e}{1 + K_L C_e} \tag{10}$$

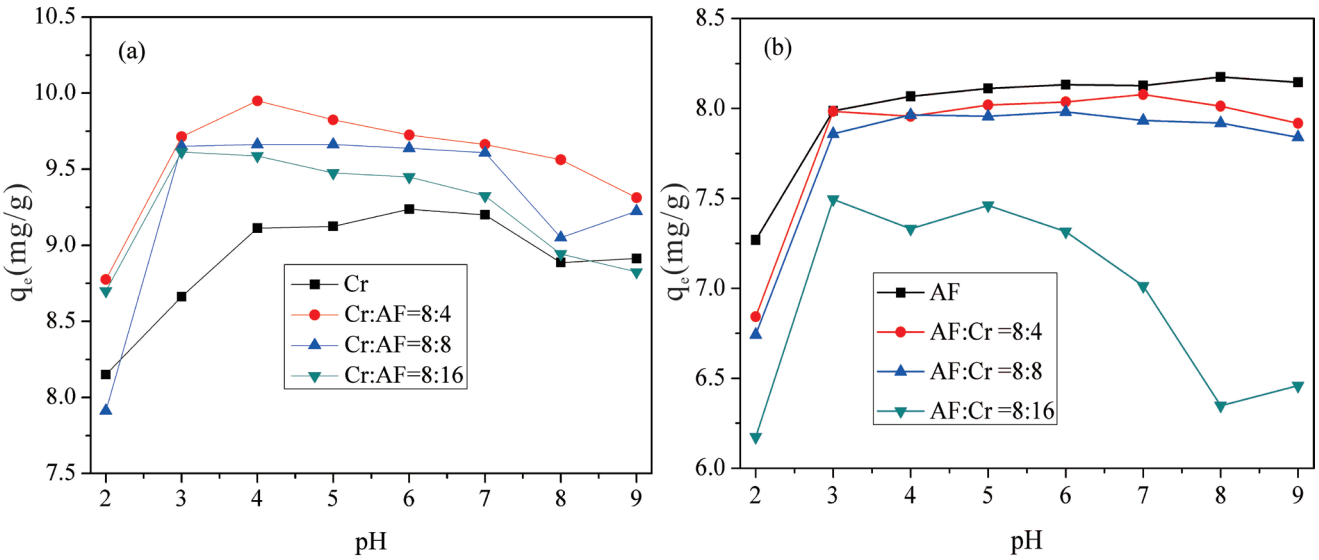

Fig. 6. Effect of Cr(VI) adsorption in the presence of AF (a) and effect of AF adsorption in the presence of Cr(VI) (b) at different pH values.

where q_m (mg/g) represents the maximum adsorption capacity of the adsorbent, K_L (L/mg) represents the Langmuir adsorption constant.

Freundlich isotherm model describes adsorption on heterogeneous surfaces or surfaces containing sites of different affinity:

$$q_e = K_F C_e^{1/n} \tag{11}$$

where K_F (mg/g) is a constant related to the relative sorption capacity of adsorbent, n is Freundlich adsorption model exponent.

The D-R model was used to evaluate the mean free energy of adsorption:

$$q_e = q_m \exp\left(-K\varepsilon^2\right) \tag{12}$$

$$\varepsilon = RT\ln\left(1+\frac{1}{C_e}\right) \tag{13}$$

$$E = \frac{1}{\sqrt{2K}} \tag{14}$$

where K (mol²/kJ²) is the relative adsorption energy constant, ε is the Polanyi potential, T (K) was the solution temperature, R was gas constant at 8.314 kJ/mol and E (kJ/mol) is the mean free energy of sorption. As usual, the value of E is used to deduce the type of sorption: if the value of E is below 8 kJ/mol, the adsorption process is physical; if the value of E is between 8 and 16 kJ/mol, it means the ion exchange happens to the adsorption process; if the value of E is above 40 kJ/mol, the adsorption process is chemical.

The Sips model is an improvement of the Langmuir model:

$$q_e = \frac{q_m a_s C_e^{1/n_s}}{1+a_s C_e^{1/n_s}} \tag{15}$$

where q_m (mg/g) was the maximum adsorption capacity of the adsorbent, a_s is the model constant and related to energy of sorption, $1/n_s$ can explain the condition of distribution of adsorption sites: if the value of $1/n_s$ is equal to 0, it means the distinction of adsorption site distribution is large and the heterogeneous sorption reaction will happen to it; if the value of $1/n_s$ is close to 0, it means the distribution of adsorption site is relatively uniform; if the value of $1/n_s$ is equal to 1, the Sips model is the same as the Langmuir.

The isotherm parameters, as well as the corresponding correlation coefficients (R^2), were listed in Table 4. The isotherm models of adsorption for Cr(VI) and AF are shown in Figs. S7 and S8 (EIS). Results indicate that the fitting of Cr(VI) adsorption to the Sips model was better than the Langmuir and Freundlich models, as indicated by the higher R^2 value. Moreover, the value of $1/n_s$ was below 1, indicating that the adsorption sites of the adsorbent surface were distributed evenly. The D-R model was also suitable for fitting Cr(VI) adsorption, as the R^2 values were all above 0.9. The values of E of D-R model at 30°C, 40°C and 50°C were 1.8866, 1.9166 and 2.0805 kJ/mol, respectively. The E values under 8 kJ/mol implied that the adsorption was a physical process. Regarding AF, it is clear that the fitting of the Sips model was better than the other isotherms, due to the higher R^2 value, which was appropriate to describe the interaction between AF molecules and BC/Cu-N. However, unlike the adsorption of Cr(VI), the values of $1/n_s$ were all above 1, which did not reflect the distribution of the adsorption sites. This was expected, as the adsorption mechanisms of AF and Cr(VI) are different. The value of E in the D-R model was below 8 kJ/mol, indicating that the adsorption of AF was a physical process.

None of the models discussed above were suitable to describe the adsorption process accurately in the binary system. In the present work, the extended Langmuir competitive multi-component model (ELMI) [49] and the extended Freundlich competitive multi-component model (EFMI) [50] were utilized to delineate the adsorption equilibrium data of the binary system.

The extended Langmuir competitive multi-component model:

$$q_i = \frac{q_{\max} K_i C_{e,i}}{1+\sum_{j=1}^{N} K_i C_{e,j}} \tag{16}$$

where q_i (mg/g) is the adsorption capacity of the i matter, $C_{e,i}$ (mg/L) is the equilibrium concentration of the i matter, $q_{\max}$ (mg/g) and K_i (L/mg) were both the model constants.

The extended Freundlich competitive multi-component model:

$$q_1 = \frac{k_{f,1} C_{e,1}^{\left(\frac{1}{n_1}\right)+x_1}}{C_{e,1}^{x_1} + y_1 C_{e,2}^{z_1}} \tag{17}$$

$$q_2 = \frac{k_{f,1} C_{e,2}^{\left(\frac{1}{n_2}\right)+x_2}}{C_{e,2}^{x_2} + y_2 C_{e,1}^{z_2}} \tag{18}$$

where $k_{f,i}$, n_1, x_1, x_2, z_1, z_2 are all the model constants.

Parameter values of the ELMI and EFMI models are given in Table 5. The binary system adsorption equilibrium data of AF and Cr(VI), as well as the predictions of the ELMI and EFMI models, are plotted in Figs. 7 and 8. As can be observed from Table 5, the values of R^2 of EFMI for AF and Cr(VI) were higher than that of ELMI, indicating that the EFMI model was more suitable to describe the binary adsorption isotherm. There were more points that presented the adsorption equilibrium data of AF and Cr(VI) falling on the fitting surface of the EFMI model, which further demonstrated that EFMI had a better fitting performance. From Fig. 8(b), the adsorption capacity of AF increased when the equilibrium concentration of Cr(VI) decreased, and vice versa. It can thus be inferred that the presence of Cr(VI) inhibited the adsorption of AF to some extent.

3.7. Kinetic studies

In order to explore the adsorption mechanism and removal efficiency of AF and Cr(VI) on BC/Cu-N, a pseudo-first-order kinetic model [51] and a pseudo-second-order kinetic model [33] were used to fit the trial data.

Table 4
Langmuir, Freundlich, D-R and Sips parameters for adsorption for Cr(VI) and AF in single system

Adsorbate	Isotherm parameters		Temperature (°C)		
			30	40	50
Cr(VI)	Langmuir	q_m (mg/g)	30.99	39.24	20.12
		K_L (L/mg)	0.4607	0.3884	0.8654
		R^2	0.8827	0.8827	0.8654
	Freundlich	K_F (mg/g)	9.5726	10.8266	8.9847
		n	1.4257	1.3116	1.9458
		R^2	0.8600	0.8563	0.7608
	D-R	q_m (mg/g)	15.78	17.94	14.50
		K (mol²/kJ²)	0.1404	0.1361	0.1150
		E (kJ/mol)	1.8866	1.9166	2.0805
		R^2	0.9096	0.9627	0.9239
	Sips	q_m (mg/g)	15.79	13.90	12.84
		a_s	1.8444	6.2774	4.1010
		$1/n_s$	0.5482	0.3064	0.3847
		R^2	0.8624	0.9954	0.9213
AF	Langmuir	q_m (mg/g)	63.13	98.35	111.10
		K_L (L/mg)	0.0598	0.0396	0.0348
		R^2	0.8362	0.80175	0.7996
	Freundlich	K_F (mg/g)	3.5689	3.7049	3.3299
		n	0.9017	0.9473	1.0078
		R^2	0.8266	0.7962	0.7500
	D-R	q_m (mg/g)	14.00	14.91	16.31
		K (mol²/kJ²)	0.6446	0.5954	0.6573
		E (kJ/mol)	0.8807	0.9164	0.8722
		R^2	0.9355	0.9027	0.8478
	Sips	q_m (mg/g)	10.61	10.77	10.78
		a_s	0.1253	0.1092	0.0421
		$1/n_s$	4.4672	5.1735	6.5947
		R^2	0.9518	0.9252	0.8757

The pseudo-first-order kinetic model has favorable effect on the equilibrium stage of the adsorption process in the initial section of the reaction:

$$q_t = q_e\left(1-10^{\frac{-k_1 t}{2.303}}\right) \tag{19}$$

The pseudo-second-order kinetic model is used to depict the whole adsorption process:

$$\frac{t}{q_t} = \frac{1}{k_2 q_e^2} + \frac{t}{q_e} \tag{20}$$

$$h = k_2\left(q_e\right)^2 \tag{21}$$

where q_t (mg/g) is the amount of adsorbate absorbed per gram adsorbent at time t; q_e (mg/g) is the amount of adsorbate adsorbed per unit mass adsorbent at equilibrium; k_1 (min^{-1}) is the rate constant of pseudo-first-order adsorption; k_2 (min^{-1}) is the rate constant of pseudo-first-order adsorption; h (mg/g min) is the initial reaction rate.

The results obtained from the fitting of experimental data to the pseudo-first-order and pseudo-second-order models for AF and Cr(VI) in single systems were described in Table 6. As shown in Fig. S9 (EIS), the two models gave an excellent adaption of the data. Whether the adsorption of AF or of Cr(VI), the fitting of pseudo-second-order model was better than pseudo-first-order model, as indicated by the higher R^2 value. For Cr(VI), it implied that there is a facilitation of electron sharing and ion exchange in the adsorption process. As can be seen, when the Cr(VI) concentration increased from 4 to 8 mg/L, the adsorption efficiency of Cr(VI) increased from 4.36 to 13.87 mg/g, which means that the adsorption capacity of Cr(VI) increased with the increase in initial concentration, under certain experimental conditions. Besides,

Table 5
Binary adsorption isotherm model parameters for Cr(VI) and AF

Adsorbate	The ELMI			The EFMI					
	K_1	K_2	R^2	$K_{f,i}$	n_i	x_i	y_i	z_i	R^2
Cr(VI)	0.00015	1085	0.8058	11.73	0.00034	–42.58	–43.43	–44.27	0.8663
AF	0.00059	–0.0767	0.3469	0.00123	0.0426	–23.11	0.00034	0.2582	0.9367

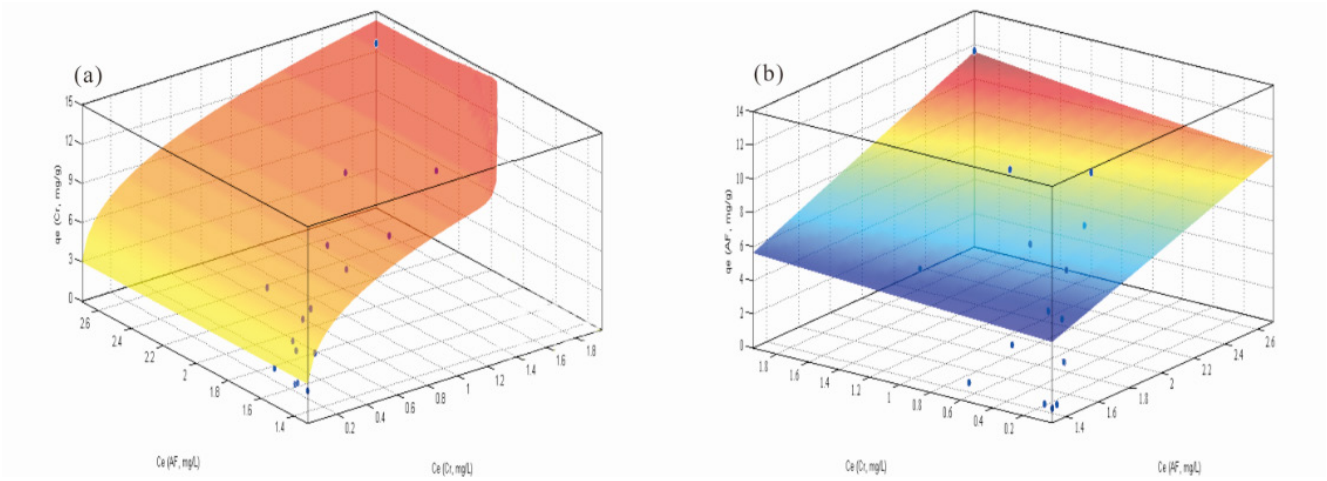

Fig. 7. ELMI isotherm model of adsorption of Cr(VI) (a) and AF (b).

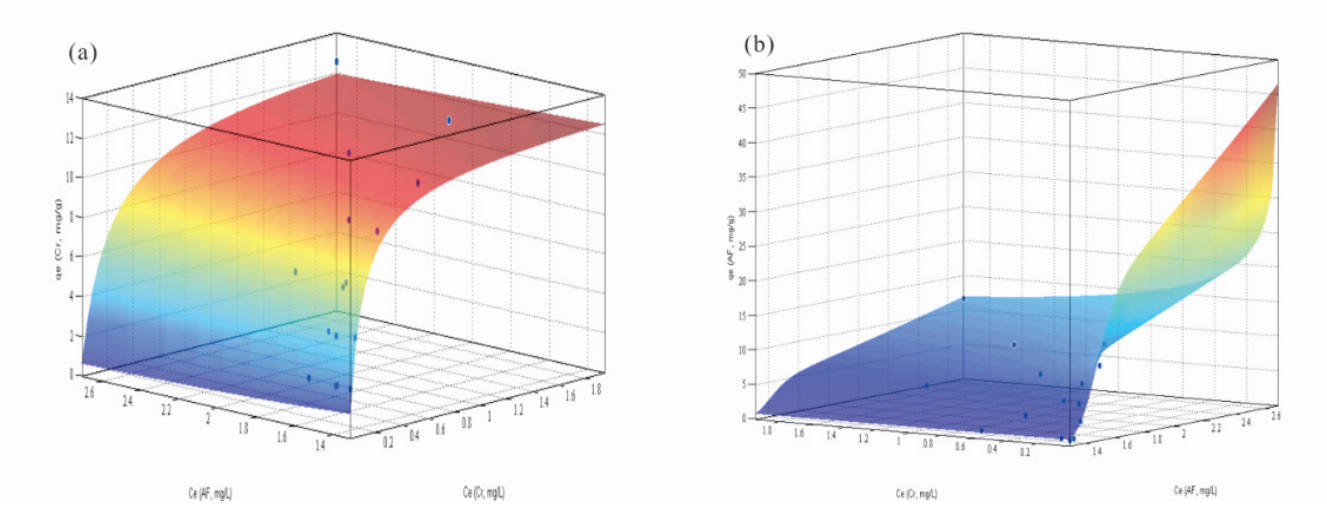

Fig. 8. EFMI isotherm model of adsorption of Cr(VI) (a) and AF (b).

the comparison of data showed that the initial reaction rate (h) was improved from 4.4653 to 18.5177 mg/g·min, with the increase in the initial concentration of Cr(VI), which was attributed to the greater diffusion rate of chromate ions in solution, resulting from the enhancement in incipient concentration. Regarding AF, the conclusion summarized from Table 6 was similar to the case of Cr(VI). The adsorption efficiency of AF was improved from 3.22 to 13.34 mg/g, with the original concentration of AF ranging from 4 to 8 mg/L, meanwhile, the initial reaction rate was increased due to the extension of the AF diffusion rate in solution.

In general, the adsorption process was divided into three stages. Firstly, it was external diffusion, which meant that the granule matter migrated through film of liquid surrounding the adsorbent. Secondly, it was intraparticle diffusion, which showed that the matter was transferred from the adsorbent surface into the internal sites. Lastly, it was the equilibrium stage, which signified that the adsorbent reached saturation and the reaction reached the equilibrium. The pseudo-second-order model provided a perfect theoretical basis for the adsorption of AF and Cr(VI), but it could not reflect the mass transfer mechanism. Hence, in this study, the Spahn

Table 6
Kinetic model parameters of adsorption of Cr(VI) and AF

Adsorbate	Kinetic parameters		C_0 (mg/L)		
			4	8	12
Cr(VI)	Pseudo-first-order	k_1	0.2552	0.2559	0.2626
		q_e (mg/g)	4.36	9.09	13.87
		R^2	0.8151	0.8876	0.9165
	Pseudo-second-order	h (mg/g min)	4.4653	10.9830	18.5177
		q_e (mg/g)	4.42	9.14	13.93
		R^2	0.9592	0.9107	0.9273
	Spahn and Schlunder	K_{ext} (1/min)	0.0087	0.0131	0.0134
		R^2	0.9388	0.9445	0.8348
	Inter diffusion	$k_{p,2}$	0.0764	0.1666	0.2322
		R^2	0.9726	0.8991	0.8746
		$k_{p,3}$	0.0022	0.1312	0.9404
		R^2	0.2009	0.3333	0.3309
AF	Pseudo-first-order	k_1	0.2370	0.1419	0.2186
		q_e (mg/g)	3.22	7.87	13.04
		R^2	0.5223	0.7741	0.8989
	Pseudo-second-order	h (mg/g min)	2.4196	2.5055	10.5098
		q_e (mg/g)	3.27	8.21	13.14
		R^2	0.9049	0.9694	0.9526
	Spahn and Schlunder	K_{ext} (1/min)	0.0024	0.0076	0.0078
		R^2	0.8819	0.9015	0.9699
	Inter diffusion	$k_{p,2}$	0.0595	0.2859	0.2933
		R^2	0.9128	0.9332	0.7958
		$k_{p,3}$	0.0031	0.0202	0.0043
		R^2	0.2811	0.0188	0.23217

and Schlunder model [52] and the intraparticle diffusion model [53] were used to fit the data obtained for a clearer transfer analysis.

The Spahn and Schlunder model is used to analyze the external diffusion process:

$$\ln C_t = \ln C_0 - k_{ext} t \tag{22}$$

where k_{ext} (1/min) is the external diffusion constant, C_0 (mg/L) is the pollutant concentration at time t. If the external diffusion in the adsorption process played a major role in the control, then $\ln C_t$ and t will show a good linear relationship; on the contrary, if there is not a great linear relationship or it exists only at a certain stage, it states the external diffusion is only the main effect factor.

The intraparticle diffusion model is used to describe the diffusion process of the contaminants within the pores of the adsorbent:

$$q_t = k_{p,t} t^{0.5} + C \tag{23}$$

where $k_{p,t}$ is the rate constant in different phases; q_t (mg/g) is the amount of substance adsorbed per unit of adsorbent at time t; C is a constant related to the thickness of boundary layer.

The fitting graph of experiment data of the Spahn and Schlunder model for AF and Cr(VI) is illustrated in Fig. S10 (EIS). The diagram showed that the adsorption of Cr(VI) and AF on the BC/Cu-N had a great linear relationship on the first 60 min and the prior 90 min, respectively. This suggests that the external diffusion had an important influence on the adsorption of Cr(VI) in the first 60 min of the reaction, and on the adsorption of AF in the first 90 min. This was combined with the results obtained from the fitting of the experimental data with the two models, as shown in Table 6. The value of k_{ext} was improved with the increase in the original concentration, which demonstrated that the improvement of the concentration extended the rate of Cr(VI) from the solution to the BC/Cu-N surface. Moreover, on the process of AF adsorption, when the AF initial concentration increased from 4 to 12 mg/L, the value of k_{ext} increased from 0.0024 to 0.0078 l/min, which proved the beneficial effect of the initial concentration on the diffusion rate. The simulated figure of adsorption, on the removal for AF and Cr(VI) is plotted in Fig. S11 (EIS). The curve obtained was divided into three sections, which did not pass through the original point, showing that the intraparticle diffusion was not the only rate-controlling process. The process could be split into three stages: first, the Cr(VI) or AF molecules diffused onto the BC/Cu-N surface and rapidly combined with the active sites; second, the adsorbate continued combining with the sites and some

Table 7
Kinetic model parameters of adsorption of Cr(VI) and AF on the binary system

Adsorbate	C_0 (mg/L)	Pseudo-first-order			Pseudo-second-order		
		k_1	q_e (mg/g)	R^2	h (mg/g min)	q_e (mg/g)	R^2
Cr(VI)	AF = 4	0.1932	9.5227	0.7975	0.0525	9.7431	0.9370
	AF = 8	0.1621	9.6318	0.9702	0.0393	9.8979	0.9306
	AF = 12	0.1603	9.3121	0.9431	0.0387	9.5877	0.9689
AF	Cr = 4	0.0978	7.7559	0.9560	0.0203	8.2036	0.9779
	Cr = 8	0.1301	7.6488	0.9124	0.0322	7.98593	0.8837
	Cr = 12	0.1205	7.2416	0.7167	0.0267	7.6307	0.9377

particles diffused inside the pores of the adsorbent, meanwhile, the improvement in concentration could promote the corresponding concentration gradient pressure and then facilitate the spread of the adsorption process, which could accelerate the sorption; third, the reaction reached dynamic equilibrium and the adsorption rate decreased considerably, as can be seen from Table 6 (the $k_{p,3}$ in three different kinds of concentration was low).

On the binary system, the parameter values of the pseudo-first-order and pseudo-second-order models for AF and Cr(VI) are described in Table 7. The fitting diagrams for the models are given in Fig. S12 (EIS). By comparing the R^2 values, the pseudo-second-order model was better to fit the adsorption of both the AF and Cr(VI). As is seen in Table 7, on the adsorption of Cr(VI), the value of h was 0.0525, 0.0393 and 0.0387 mg/g·min, when the AF concentration was 4, 8 and 12 mg/L, respectively. This indicated that the existence of AF had a negative impact on the sorption rate of Cr(VI). Regarding the AF, the value of q_e increase from 8.2036 to 7.6307 mg/g, with the concentration of Cr(VI) ranging between 4 and 8 mg/L in the coexistence system, meaning that the presence of Cr(VI) restrained the sorption of AF.

4. Conclusion

The BC/Cu-N was found to be an efficient adsorbent for the removal of AF and Cr(VI) from aqueous solutions. FTIR, XRD, SEM and EDS results demonstrated that Cu^{2+} and 3-aminopropyltrimethoxysilane were successfully loaded on the BC. RSM by CCD model was appropriate for determining the optimal conditions for AF and Cr(VI) adsorption onto BC/Cu-N. The initial concentration and adsorbent dosage were important factors for the adsorption of AF and Cr(VI), with the former having a positive correlation with the adsorption capacity, while the latter was negatively related to the adsorption efficiency. Temperature and pH had little influence on adsorption. Moreover, the isotherm investigation in a single component system revealed that the Sips model fitted both data of AF and Cr(VI) adsorption better. The maximum adsorption of AF and Cr(VI) was indicated as 13.6675 and 9.4000 mg/g, respectively. In addition, the kinetic data fitted better to the pseudo-second-order kinetic model than pseudo-first-order one, for the removal of both AF and Cr(VI). External diffusion controlled the initial process and intraparticle diffusion dominated the mass transfer process. In the binary system, the presence of AF promoted the adsorption capacity of Cr(VI). On the contrary, the presence of Cr(VI) constricted the adsorption of AF in solution. Moreover, the pseudo-second-order model was discovered to depict the binary system well. The EFMI model was more suitable than the ELMI model to describe the adsorption of both AF and Cr(VI).

Acknowledgements

This work was supported by A Project Funded by the Priority Academic Program Development of Jiangsu Higher Education Institutions.

References

[1] R.-S. Juang, H.-C. Kao, W. Chen, Column removal of Ni (II) from synthetic electroplating waste water using a strong-acid resin, Sep. Purif. Technol., 49 (2006) 36–42.
[2] R. Sharma, B. Singh, Removal of Ni (II) ions from aqueous solutions using modified rice straw in a fixed bed column, Bioresour. Technol., 146 (2013) 519–524.
[3] C.E. Barrera-Díaz, V. Lugo-Lugo, B. Bilyeu, A review of chemical, electrochemical and biological methods for aqueous Cr (VI) reduction, J. Hazard. Mater., 223 (2012) 1–12.
[4] T. Robinson, B. Chandran, P. Nigam, Removal of dyes from a synthetic textile dye effluent by biosorption on apple pomace and wheat straw, Water Res., 36 (2002) 2824–2830.
[5] A. Azhdarpoor, R. Nikmanesh, F. Khademi, A study of Reactive Red 198 adsorption on iron filings from aqueous solutions, Environ. Technol., 35 (2014) 2956–2960.
[6] C. Jain, M. Sharma, Adsorption of cadmium on bed sediments of river Hindon: Adsorption models and kinetics, Water Air Soil Pollut., 137 (2002) 1–19.
[7] A. Pagana, S. Sklari, E. Kikkinides, V. Zaspalis, Microporous ceramic membrane technology for the removal of arsenic and chromium ions from contaminated water, Micropor. Mesopor. Mater., 110 (2008) 150–156.
[8] H. Al Abdulgader, V. Kochkodan, N. Hilal, Hybrid ion exchange–Pressure driven membrane processes in water treatment: A review, Sep. Purif. Technol., 116 (2013) 253–264.
[9] M. Chérif, I. Mkacher, L. Dammak, A.B. Salah, K. Walha, D. Grande, V. Nikonenko, Water desalination by neutralization dialysis with ion-exchange membranes: Flow rate and acid/alkali concentration effects, Desalination, 361 (2015) 13–24.
[10] Y.S. Dzyazko, A. Mahmoud, F. Lapicque, V. Belyakov, Cr (VI) transport through ceramic ion-exchange membranes for treatment of industrial wastewaters, J. Appl. Electrochem., 37 (2007) 209–217.
[11] W.-q. Wang, M.-y. Li, Q.-x. Zeng, Thermodynamics of Cr (VI) adsorption on strong alkaline anion exchange fiber, Trans. Nonferrous Met. Soc. China, 22 (2012) 2831–2839.
[12] V. Khandegar, A.K. Saroha, Electrocoagulation for the treatment of textile industry effluent – a review, J. Environ. Manage., 128 (2013) 949–963.

[13] A. Mahmoud, A. Ghaly, M. Brooks, Removal of dye from textile wastewater using plant oils under different pH and temperature conditions, Am. J. Environ. Sci., 3 (2007) 205–218.
[14] S. Song, J. Fan, Z. He, L. Zhan, Z. Liu, J. Chen, X. Xu, Electrochemical degradation of azo dye CI Reactive Red 195 by anodic oxidation on Ti/SnO_2–Sb/PbO_2 electrodes, Electrochim. Acta, 55 (2010) 3606–3613.
[15] A. Tehrani-Bagha, N. Mahmoodi, F. Menger, Degradation of a persistent organic dye from colored textile wastewater by ozonation, Desalination, 260 (2010) 34–38.
[16] H. Wang, X.-W. Zheng, J.-Q. Su, Y. Tian, X.-J. Xiong, T.-L. Zheng, Biological decolorization of the reactive dyes Reactive Black 5 by a novel isolated bacterial strain *Enterobacter* sp. EC3, J. Hazard. Mater., 171 (2009) 654–659.
[17] I. Ali, M. Asim, T.A. Khan, Low cost adsorbents for the removal of organic pollutants from wastewater, J. Environ. Manage., 113 (2012) 170–183.
[18] D. Mohan, K.P. Singh, V.K. Singh, Wastewater treatment using low cost activated carbons derived from agricultural byproducts—a case study, J. Hazard. Mater., 152 (2008) 1045–1053.
[19] F.Y. Wang, H. Wang, J.W. Ma, Adsorption of cadmium (II) ions from aqueous solution by a new low-cost adsorbent—Bamboo charcoal, J. Hazard. Mater., 177 (2010) 300–306.
[20] K.-S. Chen, W.-Y. Chen, S.-C. Liao, Y.-T. Haung, S.-C. Chen, H.-R. Lin, F.-H. Lin, Surface graft polymerization acrylic acid onto bamboo charcoal and to improve ammonia adsorption, Desal. Wat. Treat., 17 (2010) 168–175.
[21] Y. Wang, X. Wang, X. Wang, M. Liu, Z. Wu, L. Yang, S. Xia, J. Zhao, Adsorption of Pb (II) from aqueous solution to Ni-doped bamboo charcoal, J. Ind. Eng. Chem., 19 (2013) 353–359.
[22] Y. Fan, B. Wang, S. Yuan, X. Wu, J. Chen, L. Wang, Adsorptive removal of chloramphenicol from wastewater by NaOH modified bamboo charcoal, Bioresour. Technol., 101 (2010) 7661–7664.
[23] M. Jain, V. Garg, K. Kadirvelu, Investigation of Cr (VI) adsorption onto chemically treated *Helianthus annuus*: optimization using response surface methodology, Bioresour. Technol., 102 (2011) 600–605.
[24] Y. Wen, Y. Wu, Optimizing adsorption of Co (II) and Ni (II) by 13× molecular sieves using response surface methodology, Water Air Soil Pollut., 223 (2012) 6095–6107.
[25] E.B. Simsek, E. Özdemir, U. Beker, Process optimization for arsenic adsorption onto natural zeolite incorporating metal oxides by response surface methodology, Water Air Soil Pollut., 224 (2013) 1–14.
[26] N. Balasubramanian, T. Kojima, C. Srinivasakannan, Arsenic removal through electrocoagulation: kinetic and statistical modeling, Chem. Eng. J., 155 (2009) 76–82.
[27] M.A. Bezerra, R.E. Santelli, E.P. Oliveira, L.S. Villar, L.A. Escaleira, Response surface methodology (RSM) as a tool for optimization in analytical chemistry, Talanta, 76 (2008) 965–977.
[28] M. Amini, H. Younesi, N. Bahramifar, Biosorption of nickel(II) from aqueous solution by *Aspergillus niger*: response surface methodology and isotherm study, Chemosphere, 75 (2009) 1483–1491.
[29] A.Ö.A. Tuna, E. Özdemir, E.B. Simsek, U. Beker, Optimization of process parameters for removal of arsenic using activated carbon-based iron-containing adsorbents by response surface methodology, Water Air Soil Pollut., 224 (2013) 1–15.
[30] V.M. Boddu, K. Abburi, J.L. Talbott, E.D. Smith, R. Haasch, Removal of arsenic (III) and arsenic (V) from aqueous medium using chitosan-coated biosorbent, Water Res., 42 (2008) 633–642.
[31] Z. Chu, W. Liu, H. Tang, T. Qian, S. Li, Z. Li, G. Wu, Surface acid–base behaviors of Chinese loess, J. Colloid Interface Sci., 252 (2002) 426–432.
[32] W. Liu, Z. Sun, W. Forsling, Q. Du, H. Tang, A comparative study of surface acid–base characteristics of natural illites from different origins, J. Colloid Interface Sci., 219 (1999) 48–61.
[33] S. Yang, Y. Wu, A. Aierken, M. Zhang, Y. Wu, Adsorption of Ni (II) using amine-functionalized MCM-41 optimized by response surface methodology, Desal. Wat. Treat., 57 (2016) 8526–8539.
[34] Y. Wu, M. Zhang, H. Zhao, S. Yang, A. Arkin, Functionalized mesoporous silica material and anionic dye adsorption: MCM-41 incorporated with amine groups for competitive adsorption of Acid Fuchsine and Acid Orange II, RSC Adv., 4 (2014) 61256–61267.
[35] G. Pugazhenthi, S. Sachan, N. Kishore, A. Kumar, Separation of chromium (VI) using modified ultrafiltration charged carbon membrane and its mathematical modeling, J. Membr. Sci., 254 (2005) 229–239.
[36] A.M. Donia, A.A. Atia, W.A. Al-amrani, A.M. El-Nahas, Effect of structural properties of acid dyes on their adsorption behaviour from aqueous solutions by amine modified silica, J. Hazard. Mater., 161 (2009) 1544–1550.
[37] N. Tewari, P. Vasudevan, B. Guha, Study on biosorption of Cr (VI) by *Mucor hiemalis*, Biochem. Eng. J., 23 (2005) 185–192.
[38] H. Li, Z. Li, T. Liu, X. Xiao, Z. Peng, L. Deng, A novel technology for biosorption and recovery hexavalent chromium in wastewater by bio-functional magnetic beads, Bioresour. Technol., 99 (2008) 6271–6279.
[39] G.D. Sheng, S.T. Yang, J. Sheng, J. Hu, X.L. Tan, X.K. Wang, Macroscopic and microscopic investigation of Ni(II) sequestration on diatomite by batch, XPS, and EXAFS techniques, Environ. Sci. Technol., 45 (2011) 7718–7726.
[40] V.C. Srivastava, I.D. Mall, I.M. Mishra, Competitive adsorption of cadmium(II) and nickel(II) metal ions from aqueous solution onto rice husk ash, Chem. Eng. Process. Process Intensif., 48 (2009) 370–379.
[41] A. Sarı, M. Tuzen, Biosorption of total chromium from aqueous solution by red algae (Ceramium virgatum): equilibrium, kinetic and thermodynamic studies, J. Hazard. Mater., 160 (2008) 349–355.
[42] S. Kizito, S. Wu, W.K. Kirui, M. Lei, Q. Lu, H. Bah, R. Dong, Evaluation of slow pyrolyzed wood and rice husks biochar for adsorption of ammonium nitrogen from piggery manure anaerobic digestate slurry, Sci. Total Environ., 505 (2015) 102–112.
[43] N. Evans, P. Warwick, T. Lewis, N. Bryan, Influence of humic acid on the sorption of uranium(IV) to kaolin, Environ. Chem. Lett., 9 (2011) 25–30.
[44] J.Y. Chen, D.Q. Zhu, C. Sun, Effect of heavy metals on the sorption of hydrophobic organic compounds to wood charcoal, Environ. Sci. Technol., 41 (2007) 2536–2541.
[45] P.R. Rout, P. Bhunia, R.R. Dash, Modeling isotherms, kinetics and understanding the mechanism of phosphate adsorption onto a solid waste: ground burnt patties, J. Environ. Chem. Eng., 2 (2014) 1331–1342.
[46] A. Babatunde, Y. Zhao, Equilibrium and kinetic analysis of phosphorus adsorption from aqueous solution using waste alum sludge, J. Hazard. Mater., 184 (2010) 746–752.
[47] Y. Wu, Y. Jin, J. Cao, P. Yilihan, Y. Wen, J. Zhou, Optimizing adsorption of arsenic (III) by NH_2-MCM-41 using response surface methodology, J. Ind. Eng. Chem., 20 (2014) 2792–2800.
[48] E.S. Dragan, D.F. Apopei Loghin, A.I. Cocarta, Efficient sorption of Cu^{2+} by composite chelating sorbents based on potato starch-graft-polyamidoxime embedded in chitosan beads, ACS Appl. Mater. Interfaces, 6 (2014) 16577–16592.
[49] A. Kurniawan, H. Sutiono, N. Indraswati, S. Ismadji, Removal of basic dyes in binary system by adsorption using rarasaponin–bentonite: revisited of extended Langmuir model, Chem. Eng. J., 189 (2012) 264–274.
[50] E. Padilla-Ortega, R. Leyva-Ramos, J. Flores-Cano, Binary adsorption of heavy metals from aqueous solution onto natural clays, Chem. Eng. J., 225 (2013) 535–546.
[51] S. Lagergren, Zur theorie der sogenannten absorption gelöster stoffe, PA Norstedt & söner, 1898.
[52] Y. Wu, J. Cao, P. Yilihan, Y. Jin, Y. Wen, J. Zhou, Adsorption of anionic and cationic dyes from single and binary systems by industrial waste lead–zinc mine tailings, RSC Adv., 3 (2013) 10745–10753.
[53] X. Mi, G. Huang, W. Xie, W. Wang, Y. Liu, J. Gao, Preparation of graphene oxide aerogel and its adsorption for Cu^{2+} ions, Carbon, 50 (2012) 4856–4864.

Supplementary information

Table S1
Experimental design in term of coded factors and the central composite design on adsorption of AF

Run order	Real (coded) values				Adsorbent capacity q_e (mg/g)
	A	B	C	D	AF
1	0	2	0	0	11.0988
2	0	0	0	0	7.2688
3	–1	1	–1	–1	11.3733
4	–1	1	1	–1	8.1460
5	0	0	0	0	7.9213
6	2	0	0	2	7.0375
7	–1	–1	1	–1	4.4210
8	0	0	0	0	7.9263
9	1	1	–1	1	10.2500
10	–1	1	–1	–1	11.2317
11	0	0	–2	0	13.6675
12	1	1	1	1	7.2480
13	0	0	0	0	7.7288
14	0	0	0	0	7.4638
15	0	0	0	0	7.6950
16	–1	–1	–1	–1	6.5667
17	1	1	1	1	7.6950
18	0	0	0	0	7.6325
19	–2	0	0	–2	5.4550
20	–1	–1	1	–1	4.4250
21	1	–1	–1	1	6.9917
22	1	–1	1	1	4.2860
23	–1	–1	–1	–1	7.1733
24	1	1	–1	1	11.0583
25	1	–1	1	1	4.5140
26	1	–1	–1	1	6.5333
27	0	0	0	0	7.5025
28	0	0	2	0	5.3333
29	0	–2	0	0	3.1838
30	–1	1	1	–1	7.6640

Table S2
Experimental design in term of coded factors and the central composite design on adsorption of Cr(VI)

Run order	Real (coded) values				Adsorbent Capacity q_e (mg/g)
	A	B	C	D	Cr(VI)
1	1	1	–1	1	8.3875
2	0	0	0	2	5.4300
3	1	–1	–1	1	4.3750
4	0	0	0	–2	5.5000
5	0	0	0	0	4.9900
6	1	–1	–1	–1	4.1125
7	1	1	1	–1	6.2000
8	1	1	1	1	6.2417
9	–1	–1	–1	–1	4.1125
10	1	1	–1	–1	8.8625
11	0	0	0	0	5.5800
12	2	0	0	0	5.3600
13	0	0	2	0	3.9786
14	–2	0	0	0	4.7300
15	–1	1	–1	1	9.4000
16	1	–1	1	1	3.0083
17	0	0	0	0	5.5600
18	0	0	0	0	5.5000
19	–1	1	1	–1	6.1500
20	0	0	0	0	5.5500
21	0	0	–2	0	8.6000
22	–1	1	1	1	6.3250
23	0	0	0	0	5.4800
24	–1	–1	1	1	3.0333
25	0	2	0	0	9.3100
26	–1	–1	–1	1	4.3875
27	0	–2	0	0	1.5800
28	–1	–1	1	–1	2.9583
29	–1	1	–1	–1	9.1500
30	1	–1	1	–1	2.9500

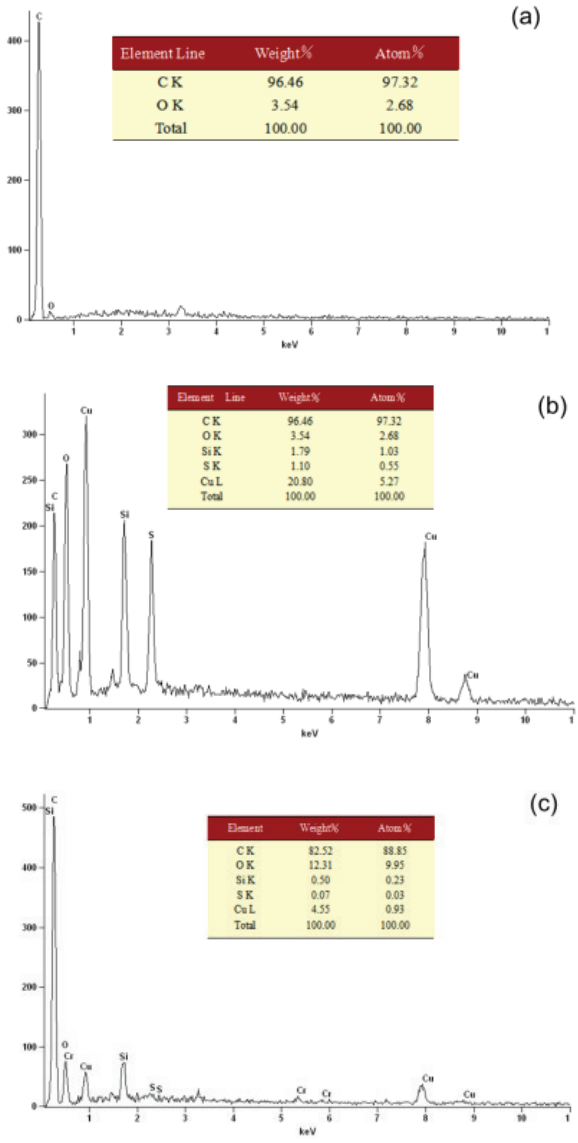

Fig. S1. EDS spectrum of BC (a), BC/Cu-N (b) and Cr(VI)-BC/Cu-N (c).

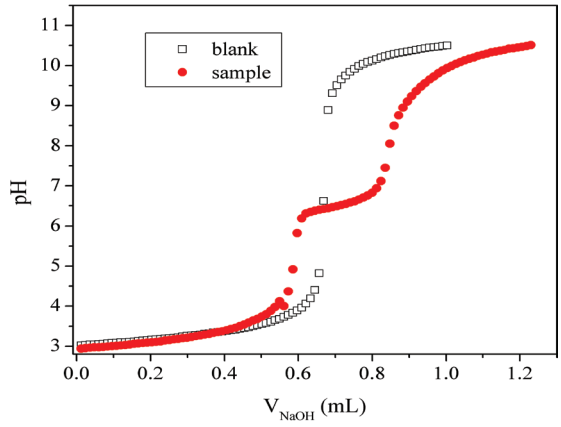

Fig. S2. Back-titration curves of BC/Cu-N.

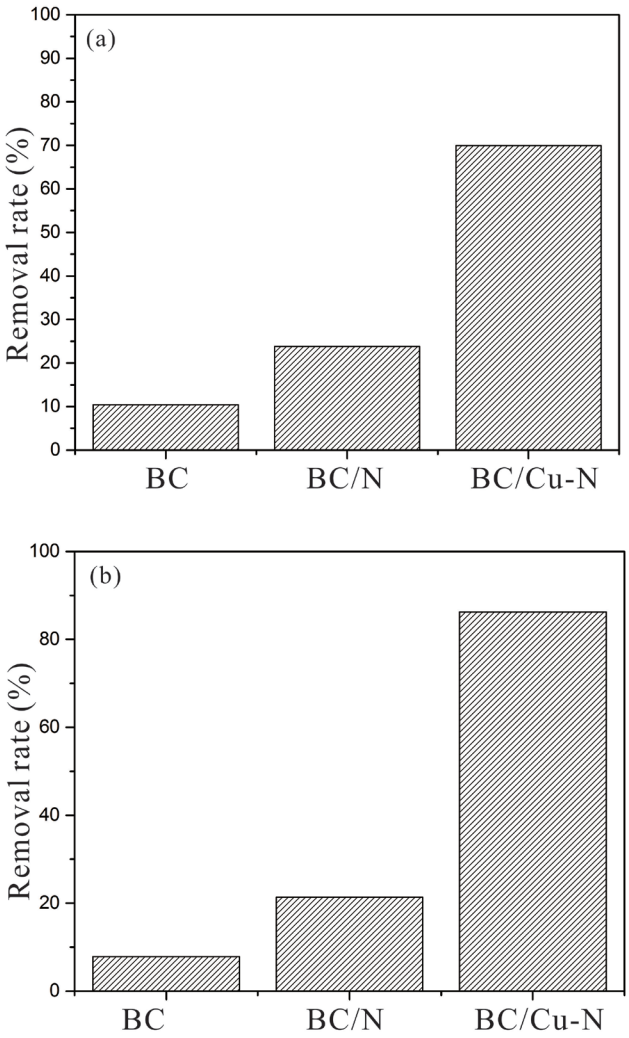

Fig. S3. Removal efficiency of Cr(VI) (a) and AF (b) by BC, BC/N and BC/Cu-N.

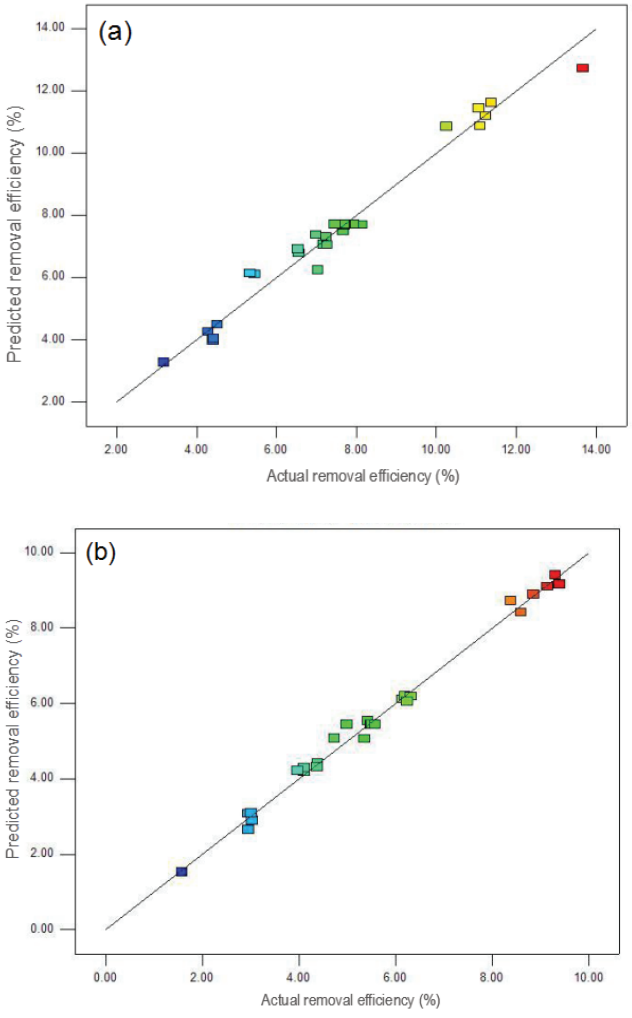

Fig. S4. Correlation of actual and predicted removal efficiency for AF (a) and Cr (b).

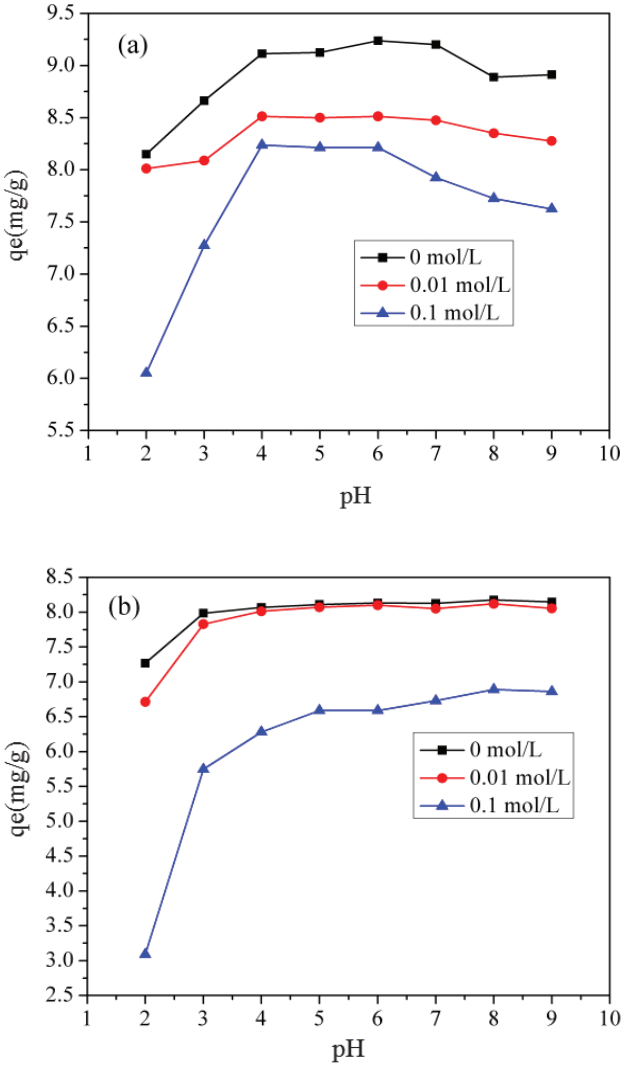

Fig. S5. The influence of pH on the adsorption of Cr (a) and AF (b).

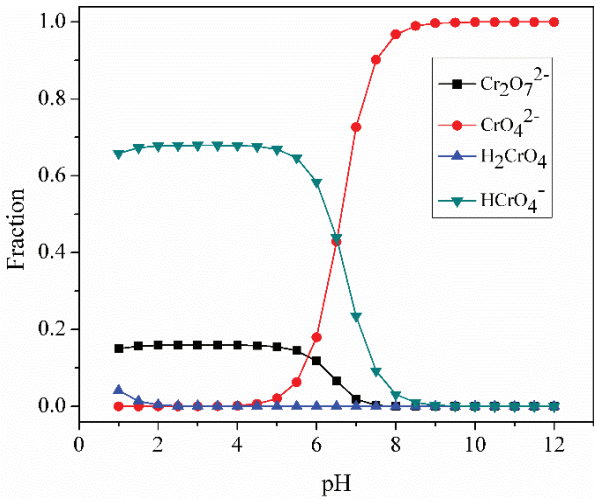

Fig. S6. The diagram of Cr(VI) chemical species in aqueous solution in different pH.

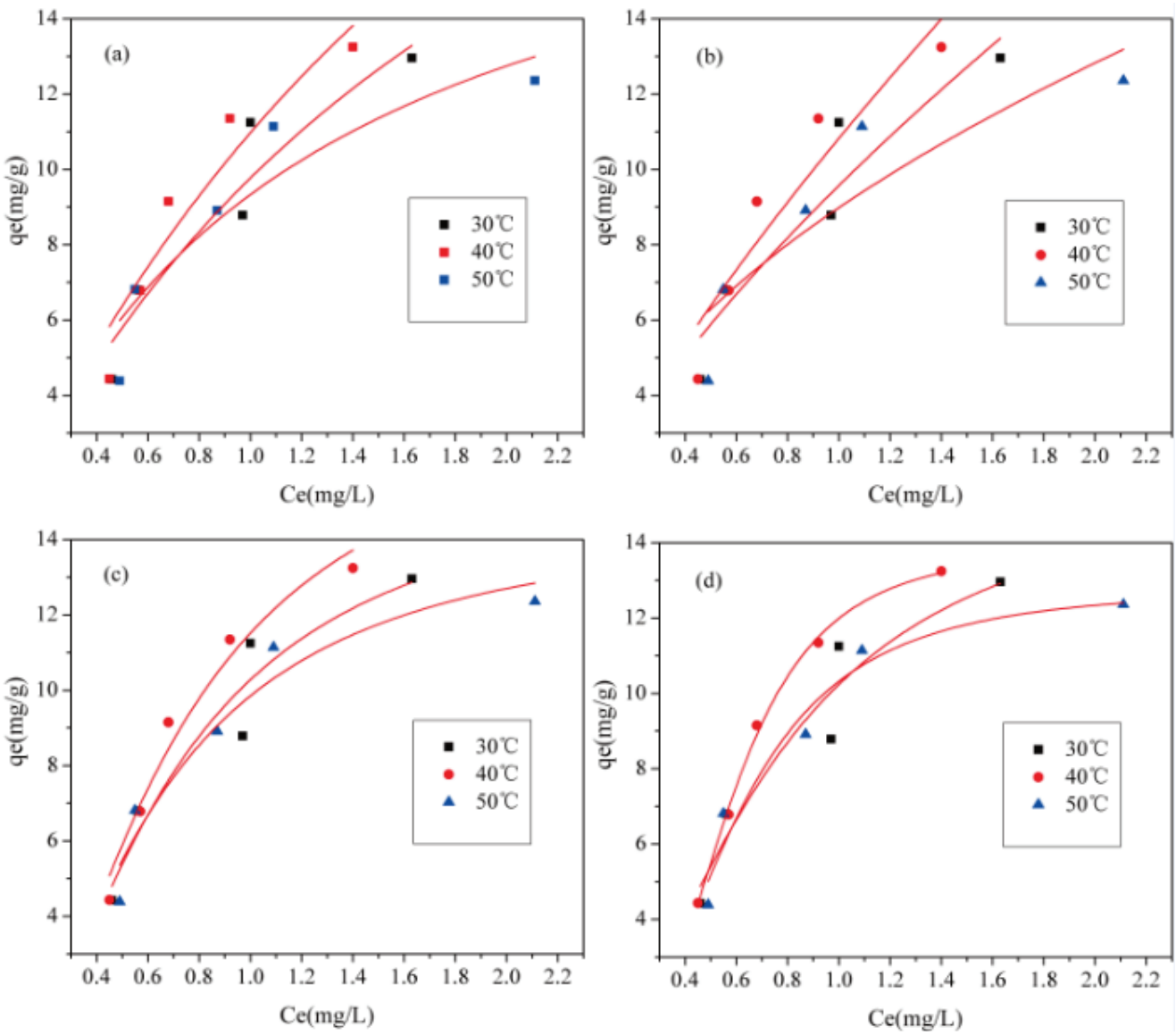

Fig. S7. Isotherm models for Cr(VI) by BC/Cu-N: (a) Langmuir isotherm model; (b) Freundlich isotherm model; (c) D-R isotherm model; (d) Sips isotherm model.

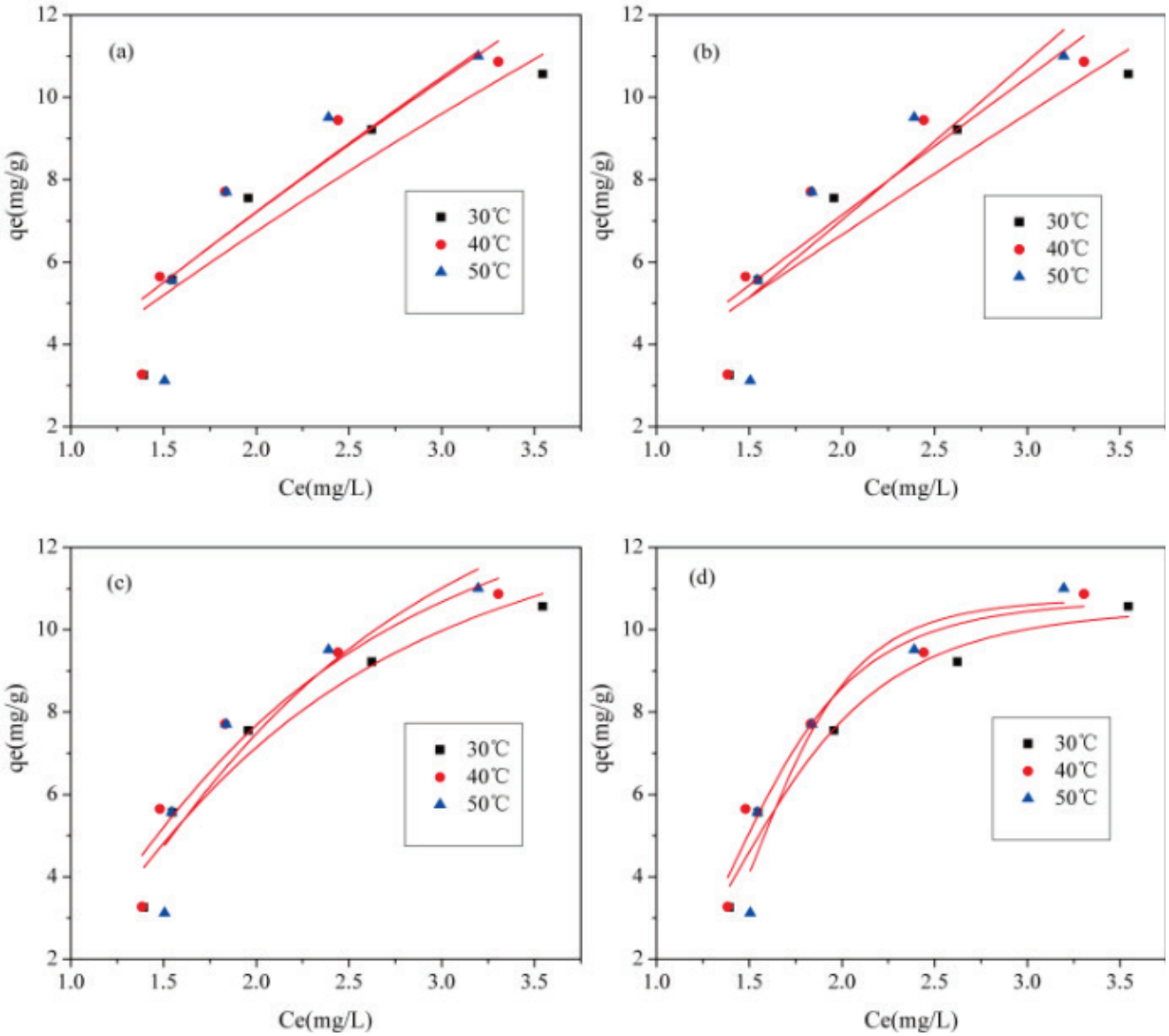

Fig. S8. Isotherm models for AF by BC/Cu-N: (a) Langmuir isotherm model; (b) Freundlich isotherm model; (c) D-R isotherm model; (d) Sips isotherm model.

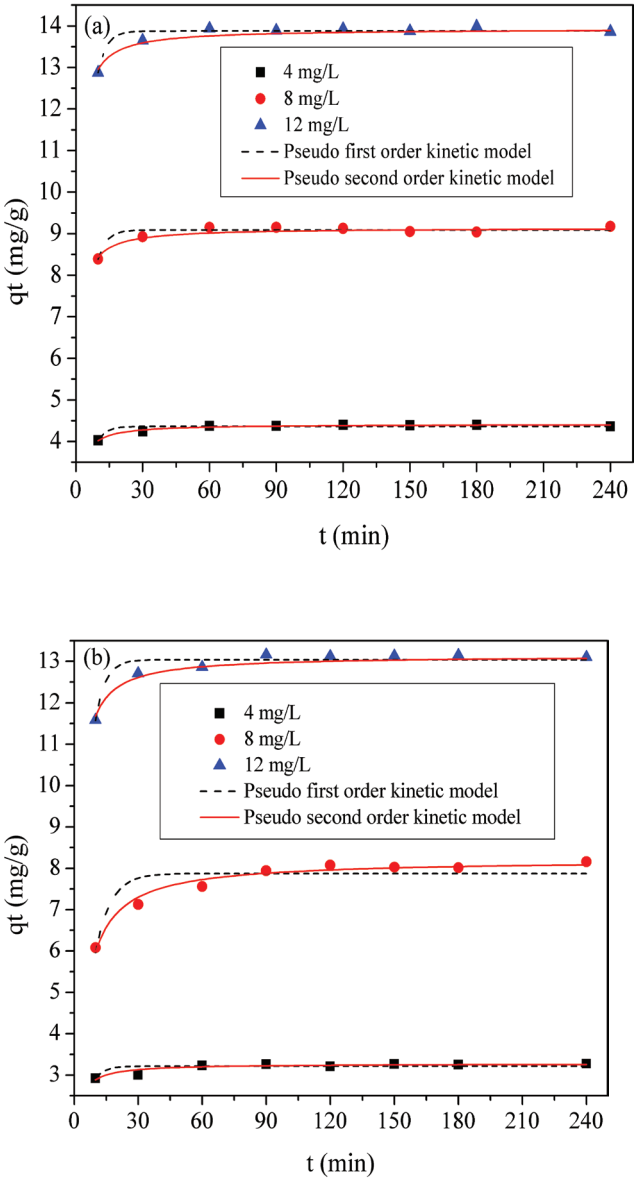

Fig. S9. Pseudo-first-order and pseudo-second-order kinetic models for Cr(VI) (a) and AF (b) in different concentrations.

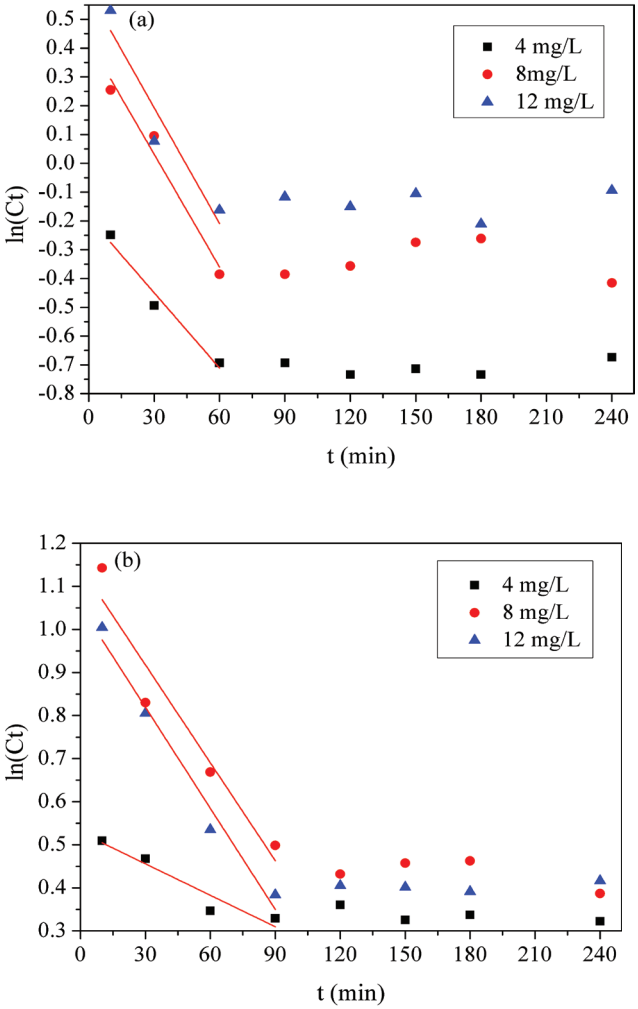

Fig. S10. Spahn and Schlunder kinetic models for Cr(VI) (a) and AF (b) in different concentrations.

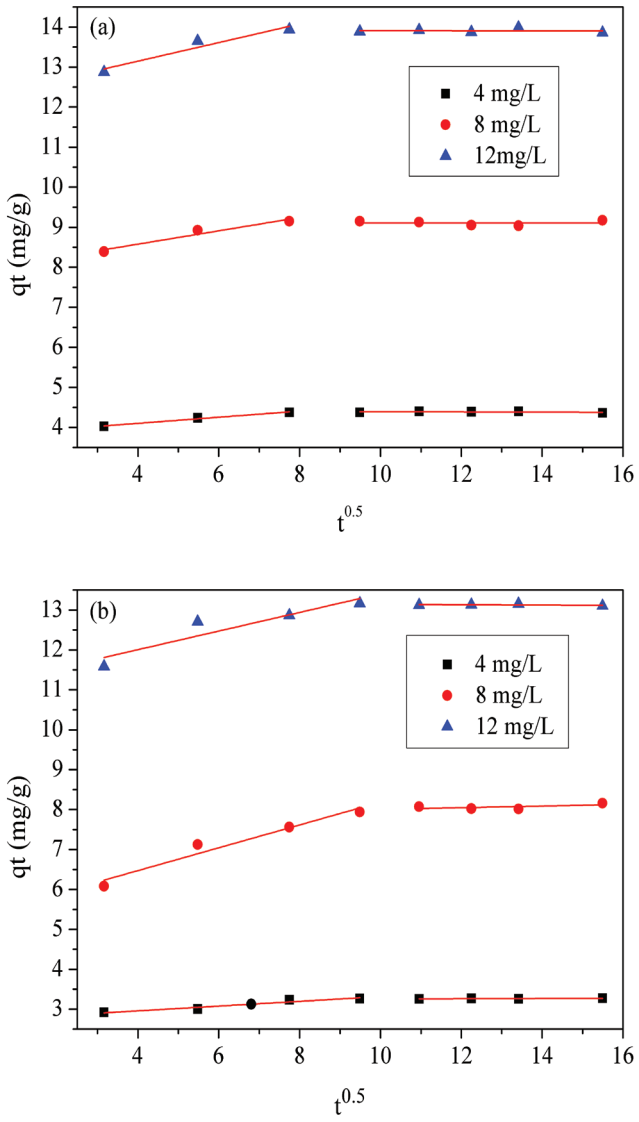

Fig. S11. Intraparticle diffusion kinetic model for Cr(VI) (a) and AF(b) under different concentrations.

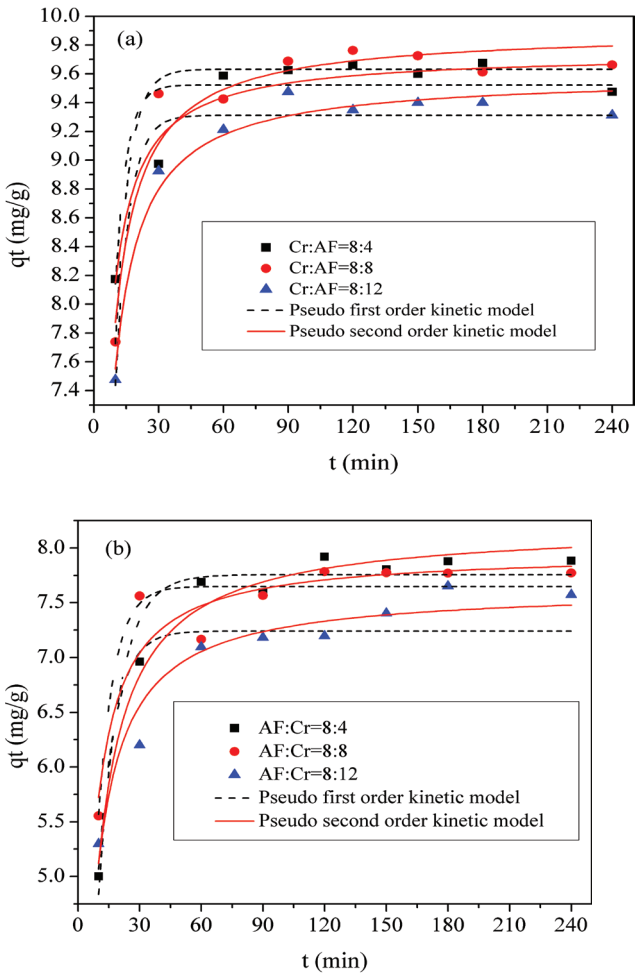

Fig. S12. On the binary system, the pseudo-first-order and pseudo-second-order kinetic models for Cr(VI) (a) and AF (b) at different concentration portions.